

Increased coherence time in narrowed bath states in quantum dots

Lars B. Gravert,* Peter Lorenz, Carsten Nase, Joachim Stolze, and Götz S. Uhrig
*Lehrstuhl für Theoretische Physik I, Technische Universität Dortmund,
Otto-Hahn Straße 4, 44221 Dortmund, Germany*

We study the influence of narrowed distributions of the nuclear Overhauser field on the decoherence of a central electron spin in quantum dots. We describe the spin dynamics in quantum dots by the central spin model. We use analytic solutions for uniform couplings and the time dependent density-matrix renormalization group (tDMRG) for nonuniform couplings. With these tools we calculate the dynamics of the central spin for large baths of nuclear spins with or without external magnetic field applied to the central spin. The focus of our study is the influence of initial mixtures with narrowed distributions of the Overhauser field and of applied magnetic fields on the decoherence of the central spin.

September 20, 2018

PACS numbers: 03.65.Yz, 72.25.Rb, 75.75.-c, 78.67.Hc

I. INTRODUCTION

In the last two decades, quantum dots have been studied intensively as realizations of quantum bits in theory¹⁻³ as well as in experiment⁴⁻⁶. In these systems, an electron or a hole is confined in all three spatial dimensions which explains the term “quantum dots”. Henceforth we address the spin of such an electron or hole as “electronic spin” or “central spin”. By suitable manipulations, this electronic spin can be controlled and prepared⁷⁻¹⁰. The central electronic spin and the spin bath given by nuclear spins of the surrounding solid are coupled by the hyperfine interaction^{2,11}. Due to this coupling the electronic spin decoheres, hence it loses its prepared initial state within a specific time scale called the coherence time. Indeed, suppressing the decoherence, i.e., prolonging the coherence time, is one of the challenging issues in the realization of quantum bits (qubits) in quantum dots. For any practical use in a quantum information device the coherence time has to be long enough to allow a certain number of logical operations applied to the quantum bit. There are various ways to suppress decoherence, i.e., to prolong the possibility of coherent manipulations. Dynamic decoupling consists of appropriate pulse sequences which can increase the coherence time significantly. Theoretical¹²⁻¹⁵ and experimental¹⁶⁻²⁰ studies have shown that dynamic decoupling is indeed a powerful strategy.

An alternative approach to enhance the coherence of the central spin is to polarize the nuclear spins coupled to the central spin²¹⁻²⁵. Due to the polarization the fluctuations of the nuclear spins are reduced and hence the central spin decoheres more slowly. According to Ref. 26, however, very high polarizations are needed to increase the coherence time significantly. The required large polarizations are not achieved in experiments so far, see Refs. 27 and 28.

A third approach to reach longer coherence consists of decreasing the fluctuations of the Overhauser field

without polarizing the nuclear spins. Theoretical²⁹⁻³³ and experimental^{8,34-37} studies present preparation techniques to realize such narrowed distributions of the Overhauser field in the initial states of the quantum dots. One crucial issue is to what extent the coherence time can be increased.

In the present paper, we will analyze the influence of different variances of the Overhauser field as well as the effect of an external magnetic field applied to the central spin. Our study is based on spin baths with about 50 to 1000 spins which are treated either analytically for uniform couplings between the central spin and all bath spins or numerically for exponentially distributed couplings.

The paper is set up as follows. First, the model is presented in Sec. II. Next, in Sec. III the two methods used are shown. In the subsequent Sec. IV the results are presented. Finally, the paper is concluded in Sec. V. Various technical aspects are explained in the appendices.

II. MODEL

We study the dynamics of an electron or hole spin in a quantum dot. This central spin is surrounded by nuclear spins. In many studies, quantum dots are composed of nuclear spins with spin quantum numbers $I > 1/2$ as they are present in Al, As, Ga, and In^{38,39}. Nonetheless we use $I = 1/2$ in our calculations for numeric simplicity.

In order to describe quantum dots, we use the central spin model (CSM) first proposed by Gaudin^{40,41}. In this minimal model, the nuclear spins are coupled to the central spin, but not directly to each other. The dipolar couplings between the nuclear spins are neglected because they are small in comparison to the dominant hyperfine couplings^{2,11}. Hence they are not important for the time scale we analyze.

In addition to the couplings between the spins we introduce an external magnetic field. This field is applied only to the central spin due to the smallness of the magnetic moment μ_{nucl} of the nuclear spins as compared to the electronic magnetic moment μ_{B} .

The considered Hamiltonian of the CSM has the form

$$\hat{H} = \sum_{k=1}^N A_k \hat{\mathbf{I}}_k \hat{\mathbf{S}} - h \hat{S}_z \quad (1a)$$

$$= \hat{\mathbf{B}} \hat{\mathbf{S}} - h \hat{S}_z \quad (1b)$$

with the central spin $\hat{\mathbf{S}}$, the magnetic field h in the z direction, the k th bath spin $\hat{\mathbf{I}}_k$, and the corresponding coupling strength J_k . The operator $\hat{\mathbf{B}}$ is the sum over all nuclear spins weighted with the corresponding coupling constant.

It is instructive to decompose the Hamiltonian according to

$$\hat{H} = \frac{1}{2} \left(\hat{B}^+ \hat{S}^- + \hat{B}^- \hat{S}^+ \right) + \hat{B}_z \hat{S}_z - h \hat{S}_z. \quad (2)$$

In this form, we can identify two parts in the Hamiltonian. The flip-flop terms $\hat{B}^+ \hat{S}^- + \hat{B}^- \hat{S}^+$ induce spin transfer between the central spin and the nuclear spins. While the z component of the total spin $\hat{S}_{\text{tot},z} = \sum_{k=1}^N \hat{I}_{k,z} + \hat{S}_z$ is a conserved quantity \hat{B}_z and \hat{S}_z separately are not constant in time. The flip-flop terms increase the decoherence of the central spin. Thus, it is desirable to suppress them. In Refs. 42–44 the influence on anisotropic couplings of a hole spin are investigated. Due to the anisotropy the flip-flop terms are suppressed. This leads to an increased coherence time. Recently, the additional effect of quadrupolar terms was considered and it was shown that it is in practice difficult to tell the various anisotropic effects apart⁴⁵.

The remaining longitudinal terms in the z direction do not change the z components but induce a Larmor precession around the z axis. The nuclear spins induce an effective field acting on the central spin called the Overhauser field, denoted by \hat{B}_z . It leads to a shift in the effective magnetic field applied to the central spin. Since the Overhauser field fluctuates the central spin dephases in its time evolution. Hence even without the flip-flop terms these fluctuations destroy the coherence of the central spin. This mechanism of dephasing is present for both hole spins and electron spins. By reducing the initial variance of the Overhauser field \hat{B}_z , i.e., by narrowing the distribution of \hat{B}_z , one expects to increase the coherence. For high magnetic fields previous papers^{29,33} showed that the coherence time is inversely proportional to the width of the distribution of the Overhauser field.

A. Couplings

The CSM can be investigated for various distributions of the couplings A_k . To compare time scales for different sets of couplings we introduce the energy scale

$$A_Q := \sqrt{\sum_{k=1}^N A_k^2}. \quad (3)$$

All energies will be expressed in units of A_Q and all times in units of $1/A_Q$ setting \hbar to unity.

Uniform couplings, i.e., $A_k = A_Q/\sqrt{N} \forall k$, are the most simple assumption. We are able to derive analytic results for this choice of couplings on the basis of previous derivations^{46,47}. We will use these results to (i) study the influence of the narrowed distributions of the Overhauser field for uniform couplings and to (ii) gauge the accuracy of the numerical DMRG data.

For a more realistic description of the couplings in quantum dots we also consider exponentially distributed couplings^{26,48,49}

$$A_k = \sqrt{\mathcal{N}} \exp\left(-k \frac{x}{N+1}\right). \quad (4)$$

This form describes the coupling constants for a localized electron in a Gaussian orbital ground state in a two dimensional quantum dot. Any other exponentially localized wave function will lead to rather similar distributions with tails of very weakly coupled spins. Since we are interested in the generic behavior but not in details of a particular system we focus on the distribution (4). The normalization factor \mathcal{N} is related to the energy scale A_Q according to

$$\mathcal{N} = A_Q^2 \frac{1 - \exp(-2x/(N+1))}{\exp(-2x/(N+1)) - \exp(-2x)}. \quad (5)$$

The spread parameter x in the exponential function determines the spread of the couplings, i.e., the ratio between the smallest and the largest coupling which is roughly given by $\exp(-x)$. For $x = 0$, the spread of the couplings is zero. Thus, we retrieve the uniform case with $\mathcal{N} = A_Q^2/N$.

B. Narrowed spin baths

We introduce a theoretical description for narrowed spin baths and investigate their effect on the dynamics of the central spin.

In previous DMRG calculations^{50–52} the initial spin bath was described by the density matrix $\hat{\rho}_b$

$$\hat{\rho}_b = \hat{\mathbf{1}}/2^N, \quad (6)$$

where $\hat{\mathbf{1}}$ is the identity operator. In this density matrix each state is obviously equally weighted. This can be justified in thermal equilibrium by the μeV energy scale of the hyperfine couplings which corresponds to fractions of a Kelvin. Thus, even at very low temperatures the nuclear spin bath will be completely disordered and all states weighted equally.

Because of the increasing interest in narrowed spin baths realized by coherent control in experimental setups³⁷ our goal is to introduce a suitable method to describe them. We introduce the density matrix

$$\hat{\rho}_b(\gamma) = \frac{1}{Z(\gamma)} \exp\left(-\gamma \hat{B}_z^2/A_Q^2\right) \quad (7)$$

for the narrowed spin baths. This density matrix provides a transparent way to describe tuned fluctuations of the Overhauser field without introducing a finite polarization. For instance, Bluhm *et al.* detect fluctuations in their double quantum dot which can be described by gaussian distributions consistently. We neglect a finite polarization of \hat{B}_z for two reasons. First, we want to focus on the reduction of the fluctuations without polarization. Second, one may shift the effect of a polarization into an externally applied static field h .

We call the parameter $\gamma > 0$ the narrowing factor because it controls the degree of reduction of Overhauser fluctuations. The partition function $Z(\gamma)$ normalizes $\hat{\rho}_b(\gamma)$; this means

$$Z(\gamma) = \text{tr} \left[\exp \left(-\gamma \hat{B}_z^2 / A_Q^2 \right) \right]. \quad (8)$$

The disordered density matrix $\hat{\rho}_b$ in (6) is restored for $\gamma = 0$. For $\gamma \rightarrow \infty$ only those states contribute which minimize \hat{B}_z^2 . Thus we expect the variance of \hat{B}_z to vanish in this limit; further details of this behavior are discussed in Sec. IV.

We assume the central spin to be prepared initially to point upwards. Then the density matrix $\hat{\rho}$ of the total CSM is initially given by the tensor product

$$\hat{\rho} = \hat{\rho}_b \otimes \left(\hat{\mathbf{1}}/2 + \hat{S}_z \right). \quad (9)$$

This assumption is the standard one. The underlying idea is that the central spin represents a quantum bit which is prepared in a special state but loses coherence subsequently due to the interaction with the bath. Of course, more subtle protocols may also induce a certain entanglement between central spin and its bath which may no longer be captured by the ansatz (9).

III. METHODS

For the analysis of the spin dynamics in the CSM we use two approaches depending on the distribution of the coupling constants A_k .

For uniform couplings we are able to derive analytic solutions for arbitrary external magnetic fields h and narrowing factors γ . For large bath sizes the analytic solution has to be evaluated numerically. Still, we can easily deal with a large number of bath spins of the order of $N \approx 10^3$. Since the numeric effort increases only quadratically with the system size we can in principle treat very large baths $N > 10^4$.

For exponentially distributed couplings we calculate the dynamics of the central spin by time dependent DMRG. This numerical method can be applied to a larger number of bath spins than most other numeric techniques; N can be as large as 10^3 , see Ref. 51. We can choose a wide range of values for the external magnetic field h , the narrowing factor γ and the coupling spread x . Since the evaluation of the analytic solution is faster than the

DMRG calculation we will use the former method for uniform couplings at $x = 0$. Additionally, we test the accuracy of the DMRG code by comparing the results of the two methods for $x = 0$.

The Bethe ansatz^{40,53} has also been used to solve the model analytically. The solutions, however, are restricted to highly polarized spin baths. Recent calculations based on the Bethe ansatz and Monte Carlo sampling^{48,49} are not restricted in that way. However the stochastic evaluation is restricted to moderately large systems of 30 to 40 bath spins in practice.

A. Analytic solutions for uniform couplings

In the uniform case the coupling constants are set to $A_k = A_Q/\sqrt{N}$ for all bath spins as noted in Sec. II A. For this choice of coupling constants we can calculate the observables analytically as presented in Refs. 46, 47, and 54. Here we briefly sketch the applied approach. By introducing the total spin $\hat{\mathbf{I}}$ of the bath, i.e., the sum over all bath spins $\hat{\mathbf{I}}_k$, we can rewrite the Hamiltonian as

$$\hat{H} = \frac{A_Q}{\sqrt{N}} \hat{\mathbf{I}} \hat{\mathbf{S}} - h \hat{S}_z. \quad (10)$$

The main advantage of the uniform case is the fact that we can treat all bath spins as one effective spin $\hat{\mathbf{I}}$. This spin is characterized by its quantum numbers j and m which correspond in the standard way to the eigenvalues $j(j+1)$ and m for $\hat{\mathbf{I}}^2$ and of \hat{I}_z , respectively. Because $\hat{\mathbf{I}}$ is composed of N spins $S = 1/2$ the maximum of j is $j_{\max} = N/2$ while its minimum is $j_{\min} = 0$ or $j_{\min} = 1/2$ for an even or odd N , respectively. The quantum number m ranges from $-j$ to j as usual.

The Hamiltonian in (1b) acts on every realization of the state $|j, m\rangle$ in the same manner. Hence it is sufficient to treat one of these realizations and to multiply the result with the degeneracy factor $\Gamma(N, j)$ which counts the number of states with given quantum numbers j and m . The factor $\Gamma(N, j)$ arises from the number of permutations to create the state $|j, m\rangle$ with N spins $S = 1/2$. For instance, there is only one way to have $|N/2, N/2\rangle$, namely all N spins are pointing up.

Using standard combinatorics and basic quantum mechanics we obtain the degeneracy factor

$$\Gamma(N, j) = \binom{N}{N/2+j} - \binom{N}{N/2+j+1} \quad (11)$$

which depends only on the number N and the quantum number j . For further details on the degeneracy factors, see Ref. 55. Here we use the definition

$$\binom{n}{k} = \begin{cases} \frac{n!}{k!(n-k)!} & k \leq n \\ 0 & \text{otherwise} \end{cases} \quad (12)$$

for the binomial coefficients.

In order to represent the density matrix $\hat{\rho}_b$ (7) in the basis spanned by the states labeled by the quantum numbers j and m , we introduce the weight $g_{j,m}(\gamma)$. This weight includes the degeneracy factor $\Gamma(N, j)$, the exponential weight $\exp(-\gamma \hat{B}_z^2/A_Q^2)$, and the partition function Z in (7). In this basis we can express the exponential weight in a particularly convenient form because it is the eigenbasis of $\hat{\mathbf{I}}$ and of the Overhauser field \hat{B}_z which is equal to \hat{I}_z times A_Q/\sqrt{N} . We easily determine the eigenvalues μ_B of \hat{B}_z to be

$$\mu_B(m) = A_Q m / \sqrt{N} \quad (13)$$

in the basis labeled by j and m . The eigenvalues are independent of the quantum number j which is helpful in calculating the partition function Z . We may carry out the sum over j explicitly obtaining

$$Z_a = \sum_{m=-N/2}^{N/2} \binom{N}{N/2+m} e^{-\gamma m^2/N} \quad (14)$$

where the sum over m remains. In principle, one can calculate Z analytically. For reasonable bath sizes N , however, we evaluate Z numerically according to (14). The weight $g_{j,m}(\gamma)$ and the density matrix $\hat{\rho}_b(\gamma)$ can be expressed as

$$g_{j,m} = \frac{\exp(-\gamma m^2/N) \Gamma(N, j)}{Z_a}, \quad (15)$$

$$\hat{\rho}_b = \sum_{j,m} g_{j,m} |j, m\rangle \langle j, m|. \quad (16)$$

To obtain the total density matrix $\hat{\rho}$ at time $t = 0$ one has to calculate the tensor product of the bath density matrix $\hat{\rho}_b$ and the density matrix $\hat{\rho}_c$ of the central spin. Here and in the following sections we assume the central spin to be polarized upwards initially.

Since we are interested in the dynamics of the system we have to determine the time evolution of the states. In the chosen basis, the Hamiltonian of the CSM is block diagonal and consists mainly of 2×2 blocks. The Hamiltonian couples the states $|\uparrow\rangle \otimes |j, m\rangle$ and $|\downarrow\rangle \otimes |j, m+1\rangle$ for $|m| < j$. The redremaining cases $|\uparrow\rangle \otimes |j, j\rangle$ and $|\downarrow\rangle \otimes |j, -j\rangle$ are eigenstates of \hat{H} . So we just have to diagonalize 2×2 blocks to compute the time evolution operator. The corresponding time dependent states and time dependent expectation values are presented in Appendix A.

B. Density matrix renormalization group

The density matrix renormalization group (DMRG) was introduced by White in 1992⁵⁶ as a method for efficient numerical renormalization in one-dimensional lattice systems. Since its introduction the DMRG has been extended to a wide range of one-dimensional systems re-

viewed in Refs. 57 and 58. In particular, it was established that DMRG is capable of capturing time dependent phenomena as well^{59,60} leading to the time dependent DMRG (tDMRG).

It was shown previously⁵¹ that tDMRG can be used to very efficiently calculate time dependent observables in the CSM for very large spin baths. By using purification, see for instance Refs. 61 and 62, we are able to directly calculate expectation values at infinite temperature. The traces are converted to expectation values of a purified state in a doubled Hilbert space. We make use of the Trotter-Suzuki decomposition (TS decomposition) in second order to evolve this purified state in time⁵¹. More explicitly, we split the Hamiltonian into local operators \hat{H}_k as follows

$$\hat{H} = \sum_{k=1}^N \left[A_k \hat{\mathbf{I}}_k \hat{\mathbf{S}} - \frac{h}{N} \hat{S}_z \right] = \sum_{k=1}^N \hat{H}_k. \quad (17)$$

These local operators act on one bath spin k and the central spin. Since we want to evolve the system iteratively in time, we define the time evolution operator

$$\hat{U} := \hat{U}(t, t + \Delta t) = \exp(-i\hat{H}\Delta t) \quad (18)$$

for a step Δt in time. With the TS decomposition we obtain

$$\hat{U} \approx \prod_{k=1}^N e^{-i\Delta t/2\hat{H}_k} \prod_{k=1}^N e^{-i\Delta t/2\hat{H}_{N+1-k}}. \quad (19)$$

This symmetric form of the short-time evolution operator (19) is correct up to Δt^3 for any Hamiltonian that can be decomposed in a sum regardless of the vanishing of the commutator $[\hat{H}_k, \hat{H}_j]$ between different local parts⁶³. To evolve the state over a finite time interval T , the number of necessary time steps is $T/\Delta t$. Thus the accumulated error of the total evolution grows like Δt^2 .

An important alternative ansatz to the TS decomposition has been introduced in Ref. 64. It is based on recursively added Krylov vectors until no substantial error in each time step occurs. Thus, no significant errors due to decomposition are introduced. The drawbacks of the Krylov approach are increased computation time and additional required memory in comparison to the TS decomposition. In Ref. 51, both approaches were carefully compared and good agreement between both methods was found unless very high accuracy is necessary. Since the central spin model can be treated quite accurately by the TS decomposition we use it for the sake of efficiency. To take the narrowed bath density matrix (7) into account we need to modify the previously used code to construct a suitable target state of the form

$$|\gamma\rangle = \exp\left(-\frac{\gamma}{2}\hat{B}_z^2/A_Q^2\right)|\psi\rangle, \quad (20)$$

where $|\psi\rangle$ is the purified state as defined in Ref. 51. For the purification, we add to each real spin of the system

an auxiliary or ghost spin which is entangled with its real counterpart in a singlet state at time $t = 0$ ⁶¹. Hence the bath state $|S\rangle$ is initially given by

$$|S\rangle = \bigotimes_{k=1}^N \frac{1}{\sqrt{2}} (|\uparrow_r \downarrow_s\rangle - |\downarrow_r \uparrow_s\rangle)_k, \quad (21)$$

where r denotes the real spin and s denotes the corresponding auxiliary spin. At $t = 0$, the purified state $|\psi\rangle$ is given by the tensor product of the bath state $|S\rangle$ and the central spin state. Since we assume the central spin to be polarized upwards the purified state reads

$$|\psi\rangle = |S\rangle \otimes |\uparrow\rangle. \quad (22)$$

With the help of the narrowed state $|\gamma\rangle$ we can calculate expectation values of any observable \hat{O} with the density matrix $\hat{\rho}$ in (9)

$$\langle \hat{O} \rangle = \text{Tr} [\hat{O} \hat{\rho}] \quad (23a)$$

$$= \frac{\langle \gamma | \hat{O} | \gamma \rangle}{\langle \gamma | \gamma \rangle} \quad (23b)$$

as shown in Ref. 61. Since one can diagonalize \hat{B}_z numerically the exponential function in (20) can be directly applied to the purified state $|\psi\rangle$. Some additional aspects must be considered because the operator \hat{B}_z consists of operators of the environment block as well as of the system block. The details of the calculation are presented in Appendix B.

Starting from the states $|\psi\rangle$ and $|\gamma\rangle$ we construct the reduced density matrix

$$\hat{\rho}'_S = \text{tr}_E [w_\psi |\psi\rangle \langle \psi| + w_\gamma |\gamma\rangle \langle \gamma|] \quad (24)$$

by tracing out the environment E . For the weights w_α we choose $w_\psi = w_\gamma = 1/2$. We sweep through the central spin system until the partition function $Z(\gamma)$ converges within some tolerance, namely the absolute difference of $Z(\gamma)$ between two consecutive sweeps is below 10^{-8} . However, the absolute difference is below 10^{-11} after the second sweep in typical cases. This partition function is easily accessed by evaluating the scalar product

$$Z_n(\gamma) = \langle \gamma | \gamma \rangle. \quad (25)$$

We observe that by adding the density matrices

$$\hat{\rho}_1 = \text{tr}_E [\hat{B}_z |\psi\rangle \langle \psi| \hat{B}_z], \quad (26a)$$

$$\hat{\rho}_2 = \text{tr}_E [\hat{B}_z |\gamma\rangle \langle \gamma| \hat{B}_z] \quad (26b)$$

to the reduced density matrix $\hat{\rho}'_S$ the numeric accuracy can be increased considerably. Therefore, we use the total reduced density matrix

$$\hat{\rho}_S = w_0 \hat{\rho}'_S + w_1 \hat{\rho}_1 + w_2 \hat{\rho}_2, \quad (27)$$

with the normalized weights $w_0 + w_1 + w_2 = 1$. In Appendix C we include an analysis to clarify how the weights w_1 and w_2 influence the accuracy of the DMRG data. We find that even small weights w_1 and w_2 increase the accuracy noticeably. Hence we choose $w_1 = w_2 = 1/22$ in the construction of the narrowed state $|\gamma\rangle$. For the tDMRG $|\gamma\rangle$ and an additional state

$$|\phi\rangle := \hat{S}_- |\gamma\rangle. \quad (28)$$

are the target states. This specific choice of (28) is due to the correlation function defined by

$$C(t) = \langle \hat{S}_+(t) \hat{S}_-(0) \rangle. \quad (29)$$

We elaborate on this correlation function in Sec. IV C. Since \hat{S}_- acts only upon the central spin we do not need to use a complete half-sweep to apply \hat{S}_- to $|\gamma\rangle$ as discussed in Ref. 59. Instead we can apply \hat{S}_- once before starting the evolution in time. We can calculate the correlation function by evaluating

$$C_n(t) = \langle \tilde{\gamma} | \hat{S}_+(t) | \tilde{\phi} \rangle \quad (30)$$

with the normalized states $|\tilde{\gamma}\rangle$ and $|\tilde{\phi}\rangle$. By this construction we can calculate correlation functions very efficiently⁵⁹.

In the following we use $m = 1024$ states in all calculations performed with the DMRG and the tDMRG. The step size is chosen as $\Delta t = 0.01 A_Q$ in all calculations performed with the tDMRG.

IV. RESULTS

With the help of the presented methods we are able to analyze the dynamics of the central spin and of the spin bath. We investigate the influence of the initial variance of the Overhauser field and of the external magnetic field applied to the central spin on the dynamics of the central spin. We deal with uniform and exponentially distributed couplings, see (4), based on the analytic solution and on the time dependent DMRG with $m = 1024$ states, respectively.

We will analyze the dependence of the variance of the Overhauser field and of the coherence time on the external magnetic field h , on the narrowing factor γ , on the spread parameter x , and on the bath size N . While all these parameters influence the initial variance and the coherence time to some degree we focus on variations in h and γ in particular because we observe the strongest dependences for them.

A. Accuracy check of DMRG

Before we turn to the variance and the dynamics we want to use the analytic results in the uniform case to deter-

mine the accuracy of the DMRG approach. We calculate the difference between the analytic results and the DMRG results for the partition function $Z(\gamma, N)$. Since this is a static quantity the difference depends only on the narrowing factor γ and the number of bath spins N , but not on the external magnetic field h . To analyze the relative error

$$\Delta Z(\gamma, N) = \left| \frac{Z_n(\gamma, N)}{Z_a(\gamma, N)} - 1 \right| \quad (31)$$

of the DMRG calculations with $m = 1024$ states we vary one parameter keeping the other constant. For the calculation of the analytic partition function Z_a and of the numeric partition function Z_n we use (14) and (25), respectively. Hence the error $\Delta Z(\gamma, N)$ measures how much the results of the DMRG calculation differs from the analytic results.

In Appendix D we present in more detail that the DMRG code is capable of describing the narrowed states for uniform couplings very well. In summary, the error ΔZ is below 10^{-11} for nearly all parameter values we considered and of the order of 10^{-9} in the worst cases. This proves the high accuracy of the DMRG code in constructing the narrowed states for $x = 0$, i.e., for uniform couplings. For nonuniform couplings the calculation becomes less accurate indicated by an increased discarded weight. Nonetheless, we are still able to calculate the narrowed states reliably as shown in the next paragraph.

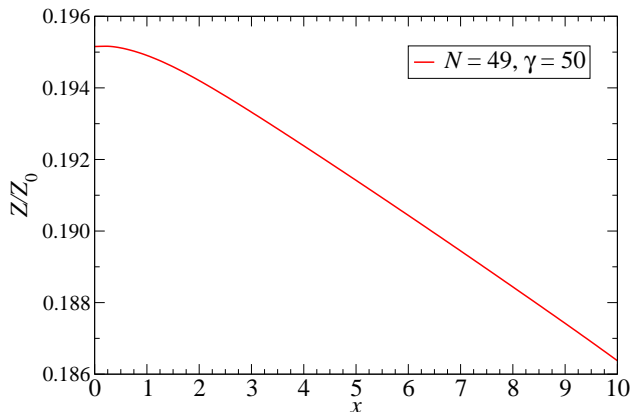


Figure 1. The relative partition function Z/Z_0 for $N = 49$ and $\gamma = 50$ depending on the spread parameter x in (4). While the spread of the couplings changes considerably according to the exponential distribution in (4) the relative partition function drops by about 5% only.

To study the dependence of Z on the spread parameter x we plot the numeric results $Z(x, \gamma)/Z_0(x)$ in Fig. IV A for a fixed narrowing factor $\gamma = 50$. Here Z_0 denotes the partition function for $\gamma = 0$. Hence the plotted quantity shows the relative reduction of the partition

function induced by the narrowing. The data shows that $Z(x, \gamma)/Z_0(x)$ depends hardly on the coupling spread x . We emphasize that the ratio between the smallest and the largest coupling in (4) is roughly given by $\exp(-x)$. Hence the case $x = 10$ captures more than four decades of coupling strengths. Nonetheless, $Z(x, \gamma)/Z_0(x)$ drops by about 5% only. For other values of $\gamma > 0$, the qualitative behavior is the same. We will also illustrate that larger values of the spread parameter x do not influence the initial variance of the Overhauser field strongly.

We conclude that we are able to construct the desired narrowed spin bath for both uniform and exponentially distributed couplings. With the DMRG approach, we can calculate various expectation values for nonuniform couplings for a wide range of the spread parameter x .

B. Initial variance of the Overhauser field

The narrowed density matrix of the spin bath in (7) leads to a reduced initial variance of the Overhauser field \hat{B}_z . The effect depends on the narrowing factor γ . To characterize the narrowed states we consider the variance σ^2 instead of γ . While these two values are connected by a one-to-one mapping as illustrated later in this section, σ^2 is a physical property of the bath while the parameter γ is a theoretical tool to tune the former. In some cases, however, it will be more convenient to use γ explicitly. Generally, the variance σ^2 is defined by

$$\sigma^2(t) = \left\langle \hat{B}_z(t)^2 \right\rangle - \left\langle \hat{B}_z(t) \right\rangle^2 \quad (32)$$

so that it depends on the bath size N , the spread parameter x , the narrowing factor γ , and the magnetic field h . Rigorously, the variance σ^2 is time dependent because the Overhauser field is not a conserved quantity. We focus on the initial variance σ^2 at $t = 0$. Otherwise, the time dependence will be denoted explicitly by $\sigma^2(t)$.

The initial variance σ^2 is independent of the magnetic field h because the field is only applied to the central spin. Hence the field h influences only the dynamics of $\sigma^2(t)$. The expectation value $\left\langle \hat{B}_z(t) \right\rangle$ vanishes at $t = 0$, so that we have the simplified initial variance

$$\sigma^2 = \left\langle \hat{B}_z^2 \right\rangle. \quad (33)$$

We study the dependence of the initial variance on the narrowing factor γ , the bath size N , and the spread parameter x . First, we discuss how σ^2 can be computed for uniform and nonuniform couplings.

By DMRG we calculate the variance σ^2 of the Overhauser field very fast and efficiently using (23b). We obtain

$$\sigma_n^2 = \frac{\langle \gamma | \hat{B}_z^2 | \gamma \rangle}{\langle \gamma | \gamma \rangle}. \quad (34)$$

The subscript ‘n’ denotes solutions calculated numerically, i.e., by DMRG. In contrast to most other methods

rather large bath sizes N can be reached for nonuniform couplings A_k in (4).

For uniform couplings we derive an analytic formula by calculating the derivative of the partition function Z . The relation

$$\sigma^2 = -A_Q^2 \partial_\gamma \ln(Z) \quad (35)$$

holds true for each spread parameter x . This can be easily concluded from the partition function Z in (8).

Since we have an analytic expression for Z in (14) for uniform couplings the variance is obtained as

$$\sigma_a^2 = A_Q^2 \sum_{m=-N/2}^{N/2} \binom{N}{N/2+m} m^2 e^{-\gamma \frac{m^2}{N}}. \quad (36)$$

The subscript ‘a’ denotes solutions calculated by this analytic formula. Since the evaluation effort increases linearly with N very large bath sizes $N > 10^4$ can be treated in this way.

Finally, we discuss the thermodynamic limit $N \rightarrow \infty$. In this limit, we are able to derive the variance $\sigma_\infty^2(\gamma)$ analytically by virtue of the central limit theorem. We obtain

$$\sigma_\infty^2(\gamma) = \frac{A_Q^2}{4 + 2\gamma} \quad (37)$$

as shown in Appendix E. With increasing bath size N , the variance $\sigma^2(\gamma)$ approaches the limit σ_∞^2 . Since the limit does not depend on the distribution of coupling constants A_k the variance $\sigma_\infty^2(\gamma)$ is valid for uniform couplings as well as for nonuniform couplings. But the bath size N for which the variance $\sigma^2(\gamma)$ can be approximated reliably by the limit $\sigma_\infty^2(\gamma)$ depends on the actual distribution of the coupling constants as we show here.

First, we investigate the influence of the narrowing factor γ on the variance. In Fig. 2 we show three variances $\sigma^2(\gamma)$ depending on γ . Two curves represent the variances for uniform couplings for $N = 49$ and $N = 50$ bath spins, respectively. The third curve represents the variance for $N = 49$ bath spins and the spread parameter $x = 1$ in (4). In addition, we plot the variance $\sigma_\infty^2(\gamma)$ of the thermodynamic limit in (37) depicted by the dashed black line.

All curves start at the same value at $\gamma = 0$. The initial value σ^2 is computed analytically for every spread parameter x . By rearranging the expectation value in (33) we obtain

$$\sigma^2 = \sum_{k,l} A_k A_l \langle \hat{I}_{z,k} \hat{I}_{z,l} \rangle \quad (38a)$$

$$= \sum_{k \neq l} A_k A_l \langle \hat{I}_{z,k} \hat{I}_{z,l} \rangle + A_Q^2/4. \quad (38b)$$

For $\gamma = 0$ the expectation value $\langle \hat{I}_{z,k} \hat{I}_{z,l} \rangle$ for $k \neq l$ vanishes because the spin operators are traceless and the

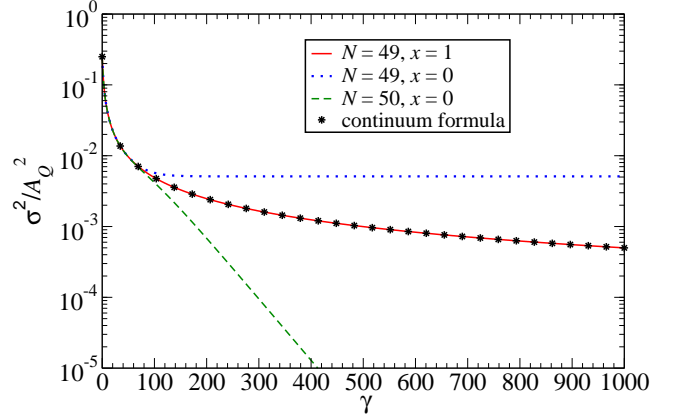


Figure 2. Variance $\sigma^2(\gamma)$ for three sets of parameters. The red solid curve is calculated for a nonuniform system with $x = 1$ and $N = 49$. It is approximated well by the thermodynamic limit (37) (black dashed curve) in the whole interval shown. A curve for $x = 1$ and $N = 50$ is not shown because it could not be distinguished from the $x = 1$ and $N = 49$ case. The blue curve is calculated for a uniform system ($x = 0$) and $N = 49$. For large values of γ the curve saturates to the value $A_Q^2/196$ according to (41). The green curve is calculated for a uniform system with $x = 0$ and $N = 50$. The curve decays as $\exp(-\gamma/N)$ for large values of γ according to (41).

density matrix of the bath spins $\hat{\rho}_b(\gamma = 0)$ is proportional to the identity matrix. Finally, we arrive at

$$\sigma^2(\gamma = 0) = A_Q^2/4 =: \sigma_0^2. \quad (39)$$

This result for $\gamma = 0$ matches with the variance σ_∞^2 of the continuum limit in (37).

For increasing values of γ the variance σ^2 decreases as shown in Fig. 2 because states with larger values for the z component of the Overhauser field are suppressed more and more. The fluctuations of the Overhauser field are a source of dephasing of the central spin. We show in the next subsection that this dephasing is suppressed as well. For not too large values of γ up to roughly 60 the variances decrease in all three cases as described by the approximate expression (37). But for even larger values of γ the three variances start to deviate from one another. The most obvious feature in Fig. 2 is the dependence of the variances for uniform couplings on the parity of the number N of bath spins. To analyze this dependence we investigate the behavior for large values of γ because in this limit the differences become most pronounced.

For large values of the narrowing factor γ the main contribution to the density matrix $\hat{\rho}_b$ arises from the states with the lowest moduli of eigenvalues $|\mu_B|$ of the Overhauser field \hat{B}_z . In the uniform case \hat{B}_z is proportional to the z component of the momentum of the bath \hat{I}_z . Thus, the eigenvalues μ_B are proportional to the eigenvalues m of \hat{I}_z . For an odd number N the eigenvalue of m with

the lowest modulus is $\pm 1/2$ while it is zero for an even number N . This difference in the lowest eigenvalues is the source of the dependence on the parity of N .

For further analysis we approximate the partition function $Z(\gamma)$ in (14) for large values of γ/N as

$$Z(\gamma) \approx \begin{cases} 2 \binom{N}{N/2+1/2} e^{-\gamma/4N} & N \text{ odd} \\ \binom{N}{N/2} \left(1 + 2 \frac{N}{N+2} e^{-\gamma/N}\right) & N \text{ even} \end{cases} \quad (40)$$

by taking only the leading order into account. Using (35) we obtain

$$\sigma^2(\gamma) \approx \begin{cases} A_Q^2/(4N) & N \text{ odd} \\ \frac{2A_Q^2}{N+2} e^{-\gamma/N} & N \text{ even} \end{cases} \quad (41)$$

for large values of the ratio γ/N . Any flip of a spin changes the eigenvalue m by 1. Since the weight for the narrowed states in (14) is proportional to $\exp(-m^2\gamma/N)$ any spin flip is exponentially suppressed.

For odd N the variance σ^2 saturates at the finite value $A_Q^2/(4N)$. Hence we are not able to decrease the fluctuations of the Overhauser field further. In contrast, the variance σ^2 decreases exponentially for even N . Thus, we can arbitrarily narrow the initial distribution of \hat{B}_z in principle. But we consider the limit of infinite ratio γ/N to be unphysical because in this limit any deviation from uniform couplings comes more and more severely into effect.

For nonuniform couplings the situation is more complex. In this case, the Overhauser field \hat{B}_z is not proportional to \hat{I}_z . Spin flips of weakly coupled spins, i.e., spins with larger index k in (4), influence the eigenvalue μ_B only weakly. Hence the suppression of states with larger values of μ_B is smoother than in the uniform case.

Increasing the bath size N leads generally to a better agreement between calculations for finite spin baths and for the thermodynamic limit $N \rightarrow \infty$. To analyze this behavior quantitatively we study the relative deviation

$$\Delta\sigma^2(N, \gamma) = \left| \frac{\sigma^2(N, \gamma)}{\sigma_\infty^2(\gamma)} - 1 \right|. \quad (42)$$

The deviation $\Delta\sigma^2(N, \gamma)$ measures how much the variance $\sigma^2(N, \gamma)$ for a finite bath size N deviates from the corresponding variance $\sigma_\infty^2(\gamma)$ in the thermodynamic limit. From the results in Fig. 2 we expect that the deviations are significantly stronger for uniform couplings than for exponentially distributed couplings. In Fig. 3, we plot the relative deviation for three values of γ depending on the bath size N for uniform couplings.

For small bath sizes $N < 50$ all three curves show large relative deviations, especially for $\gamma \geq 100$. In addition, we observe jumps in $\Delta\sigma^2$ for consecutive values of N resulting from the dependence on the parity of the bath size N . These observations support the analysis of the data displayed in Fig. 2. With increasing bath size N the relative deviations decrease. In an intermediate range of bath sizes $\Delta\sigma^2$ no longer shows a strong dependence

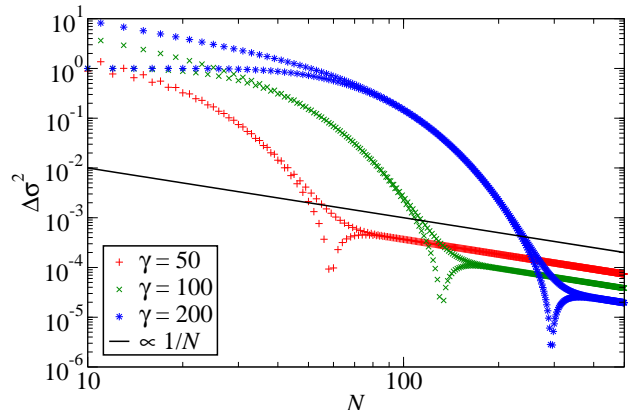


Figure 3. Relative deviation $\Delta\sigma^2$ defined in (42) depending on N for three different values of the narrowing factor γ and uniform couplings ($x = 0$). The black line depicts the power law $\propto 1/N$; note the doubly logarithmic scale.

on the parity of N . The position of this range differs depending on the value of γ . Lower values of γ push this range to lower bath sizes N . For sufficiently large bath sizes N the deviation $\Delta\sigma^2$ decreases approximately like $1/N$ for all three values of γ .

In Fig. 3, we observe a dip like feature in $\Delta\sigma^2$ in the baths with even number of spins. This dip is accompanied by a cusp like change of the slope for even and odd N . This feature appears for all values of γ . The position N_{dip} of the dip depends on γ . The three curves in Fig. 3 suggest a relation $N_c \propto \gamma$. The dip signals a crossing of $\sigma^2(N, \gamma)$ and $\sigma_\infty^2(\gamma)$ so that $\Delta\sigma^2(N, \gamma)$ becomes very small, but since the bath size N is discrete, it does not vanish completely. Still one can define a characteristic even N_c where the crossing takes place. For any finite odd bath size N_{odd} the variance $\sigma^2(N_{\text{odd}}, \gamma)$ lies higher than $\sigma_\infty^2(\gamma)$. In addition, one can define a crossing value γ_c for any given even bath size N fulfilling

$$\Delta\sigma^2(N, \gamma_c) = 0. \quad (43)$$

We call the corresponding variance the crossing variance and denote it by $\sigma_c^2(N)$. Since the deviation $\Delta\sigma^2$ vanishes for γ_c we find for the crossing variance

$$\sigma_c^2(N) = \frac{A_Q^2}{4 + 2\gamma_c} = \sigma_\infty^2(\gamma_c). \quad (44)$$

Inspecting Fig. 3 we see that the bath size N_c of the crossing variance also indicates the lowest bath size above which the variance of the Overhauser field does no longer display sizable finite size effects. In other words, for systems larger than N_c the approximate formula (37) works well.

In Fig. 4 we plot the crossing variance for uniform systems. From this figure, we conclude that large bath sizes N are required to study narrowed spin baths.

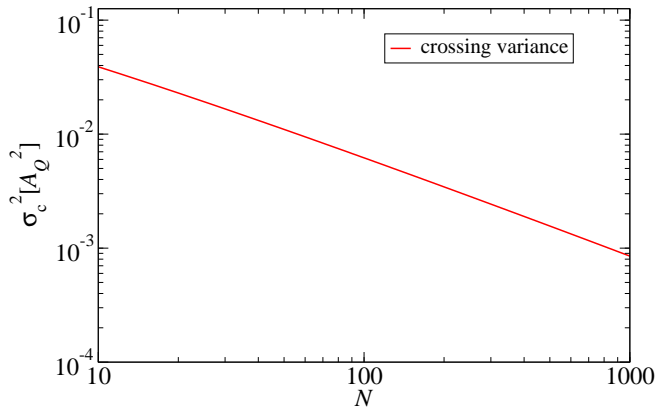


Figure 4. Crossing variance σ_c^2 defined in (44) depending on the bath size N for uniform couplings. This variance represents the lowest variance for which the uniform system does not show significant finite size effects.

In the case of nonuniform couplings with spread parameter $x = 1$ the deviation $\Delta\sigma^2$ behaves quite differently. In Fig. 5 we plot three curves for the same values of γ as in Fig. 3. Note that the curves start at values two orders of magnitude lower than in the uniform case. For small bath sizes $N < 30$, we still observe some dependence of $\Delta\sigma^2$ on the parity of the N . Then, however, the curves quickly follow the power law $\propto 1/N$, i.e., they become independent of the parity of N . These results corroborate our above argument that nonuniform couplings dampen the finite size effects of the bath.

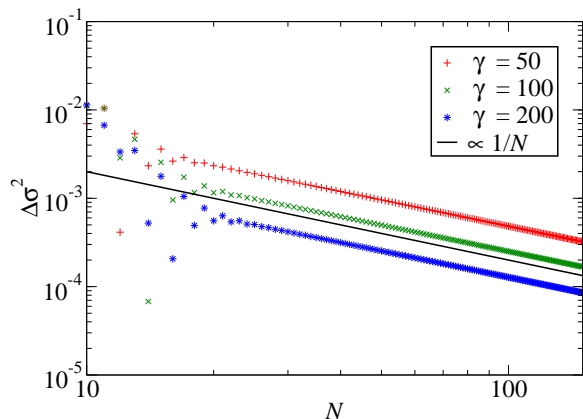


Figure 5. Relative deviation $\Delta\sigma^2$ in (42) depending on N for three different values of the weight factor γ and nonuniform couplings with the spread parameter $x = 1$. The black line is a power law $\propto 1/N$.

We conclude that for uniform and for nonuniform cou-

plings we can find sufficiently large baths $N > N_c$ such that the behavior of the system depends hardly on N . Hence we do not need to investigate the influence of N on the coherence time in the next subsection because we choose N large enough to observe the thermodynamic limit essentially.

Finally, we study the influence of the spread parameter x on the variance. In Fig. 6 the variance σ^2 and its dependence on the coupling parameter x is depicted. We have chosen four bath sizes $N = 49$, $N = 50$, $N = 99$, and $N = 100$ to capture a possible dependence of σ^2 on the parity N as discussed before. The narrowing factor is $\gamma = 200$. The variances σ^2 quickly approach the thermodynamic variance $\sigma_\infty^2(\gamma = 200) = A_Q^2/404$. For spread parameters $x > 0.6$, there is no visible difference between the variances for $N = 49$ and $N = 50$. For larger bath sizes $N = 99$ and $N = 100$ the variances converge faster to the thermodynamic variance. For $x > 0.4$ the corresponding curves already show no visible difference. For even larger bath sizes the variances will converge even faster so that for $N > N_c$ even for $x = 0$ we are still able to capture the physics of the thermodynamic variance if $\gamma < \gamma_c$. In this limit the variance is indeed almost independent of the spread parameter x .

Due to the saturation the spread parameter x influences the variance σ^2 only weakly once we reach a certain threshold. The exact value depends on the bath size N and the narrowing factor γ . For sufficiently large bath sizes even uniform couplings can be chosen to analyze the coherence time as discussed before in this section. To calculate the coherence time we will choose a large bath size N and uniform couplings, i.e., $x = 0$ as well as a smaller bath size N and nonuniform couplings with a spread parameter of $x = 1$.

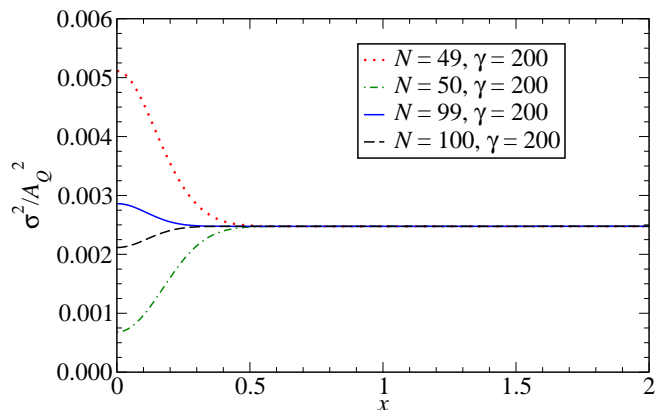


Figure 6. Variance σ^2 for the narrowing factor $\gamma = 200$ and four bath sizes N depending on the spread parameter x . Both curves quickly reach the thermodynamic limit $\sigma_\infty^2(\gamma = 200) = A_Q^2/404$ according to (37).

C. Decoherence

The central spin is prepared initially to be polarized upwards. Due to the interaction in the Hamiltonian (1b) the central spin decoheres in the course of its temporal evolution. We call the characteristic time scale for which the central spin keeps its initial state the ‘‘coherence time’’. One of the crucial goals of quantum information processing is to maintain coherence as long as possible. Thus, we aim at long coherence times.

To analyze the dependence of the coherence time on the initial variance σ^2 in (33) of the Overhauser field \hat{B}_z and the external magnetic field h in the Hamiltonian (1b) we introduce the correlation function

$$C(t) = \langle \hat{S}_+(t)\hat{S}_-(0) \rangle. \quad (45)$$

Since the central spin is fully polarized upwards for $t = 0$ one has $C(0) = 1$. In its temporal evolution the modulus $C(t)$ decreases and decays towards zero. By narrowing the variance σ^2 this decay is slowed down as shown in this section.

We define the coherence time T_2 by the relation

$$|C(T_2)| = e^{-1}. \quad (46)$$

For nonuniform couplings, we calculate $C(t)$ for equidistant time steps iteratively by tDMRG and determine T_2 by linear interpolation between these time steps. For uniform couplings we can evaluate (45) at arbitrary time t , see (A11a) and (A11b). Hence root-finding methods can be used to find the instant fulfilling (46). Note that the key idea of using the correlation (45) is to eliminate the main effect of Larmor oscillations about the z axis.

While $C(t)$ decreases in time, it still shows some oscillations remaining from the Larmor precession depending on the external magnetic field h . Since we define the coherence time by a threshold it may happen that T_2 jumps for particular fields from one maximum of the oscillation to the next. Increasing h shifts the maximum to lower times so that the coherence time decreases until it jumps to the next maximum. Due to this behavior the graphs $T_2(\sigma^2)$ and $T_2(h)$ display sawtooth like features which are superposed to the overall trend of decay. The sawtooth behavior is an artifact of our way to determine T_2 ; but it does not conceal the overall behavior.

For high magnetic fields we can derive an analytic solution for the correlation function $C(t)$ in the thermodynamic limit $N \rightarrow \infty$. Neglecting the flip-flop terms yields

$$C_\infty(t) = \exp\left(-\frac{\sigma_\infty^2 t^2}{2} + iht\right) \quad (47)$$

for the correlation function with the variance σ_∞^2 in (37). In Appendix F we present the calculation in detail. The coherence time in this limit reads

$$T_{2,\infty} = \sqrt{2}/\sigma_\infty. \quad (48)$$

The coherence time $T_{2,\infty}$ in the high-field limit can be increased arbitrarily by reducing the initial variance σ_∞^2 (γ). Without narrowing, i.e., for $\sigma^2 = A_Q^2/4$, our result is consistent with previous papers. For instance in Ref. 65, Eq. (10) describes the same coherence time; it is denoted by T_2^* there. In Ref. 33 the coherence time T_2 is calculated in the presence of a narrowed Overhauser field and strong magnetic field with the same result as ours.

In the subsections below, we analyze the effects of the initial variance σ^2 and of the external magnetic field h on the coherence time T_2 . In the previous subsection, we showed that the spread parameter x and the bath size N hardly influence the variance σ^2 for suitable ranges of parameters, i.e., $N > N_c$ and x not too small. Hence the coherence time T_2 is nearly independent of these parameters as well; it changes only by a few percent at most. Thus we restrict ourselves to two representative sets of parameters: (i) exponentially distributed couplings with $x = 1$ and $N = 49$ and (ii) uniform couplings and $N = 999$ bath spins. For these parameter sets the coherence time T_2 is mainly influenced by the initial variance σ^2 and the magnetic field h .

Since the truncation error of the tDMRG grows over time, see Ref. 51, we need to decide up to which truncation error we can consider the calculated data reliable. The truncation error arises from the discarded weight in the DMRG steps, and it grows exponentially in time⁶⁶. It is not due to the Trotter-Suzuki decomposition which constitutes also a source of a systematic error, but is much better controllable⁵¹.

To quantify the truncation error of the tDMRG we choose the accumulated discarded weight

$$\varepsilon_{\text{acc}} = \sum_j \varepsilon_j = \sum_j \left(1 - \sum_n w_{j,n}\right), \quad (49)$$

which is the sum of all discarded weights ε_j of the j th step in the tDMRG⁵¹. Another suitable measure is the accumulated discarded entropy⁶⁷

$$S_{\text{trunc}} = \sum_j S_{\text{trunc},j} = \sum_j \left(-\sum_n w_{j,n} \log(w_{j,n})\right), \quad (50)$$

which is the sum of all discarded entropies $S_{\text{trunc},j}$ of the j th step in the tDMRG. In our calculations S_{trunc} behaves qualitatively very similar to $-\varepsilon_{\text{acc}} \log(\varepsilon_{\text{acc}})$. Hence we finally choose ε_{acc} for numerical simplicity.

For the accumulated discarded weight ε_{acc} we choose the threshold error $\varepsilon_{\text{th}} = 10^{-3}$. If ε_{acc} exceeds this value we do not push the calculation further. The time instant at which this happens is dubbed the threshold time t_{th} . Depending on the variance σ^2 and on the magnetic field h we are able to reach different values of t_{th} . For times $t > t_{\text{th}}$ the data from the DMRG calculations are not reliable so that we are not able to calculate the coherence times T_2 larger than t_{th} . This occurs especially for small variances σ^2 and/or small magnetic fields h . But we emphasize

that the accumulated discarded weight is well below 10^{-5} for $t = T_2$ except for special cases.

Furthermore, we are limited by the required CPU time. Hence we do not investigate time scales $A_Q t > 40$.

1. Dependence of the coherence time on the initial variance

In Fig. 7, we plot $T_2(\sigma^2)$ for various magnetic fields h depending on σ^2 . In addition, the corresponding coherence time T_2 is depicted in the high-field limit (48). The curves computed for uniform and nonuniform couplings almost coincide. This observation agrees with previous works^{44,47} stating that the short-time dynamics depends hardly on the distribution of the coupling constants A_k . For all magnetic fields h , the coherence time T_2 increases for decreasing variance σ^2 as expected. We observe, however, a qualitative difference between the curves for $h = 0.1A_Q$ and for $h = 3A_Q$ or $h = 10A_Q$. We discuss the low-field and high-field regimes separately.

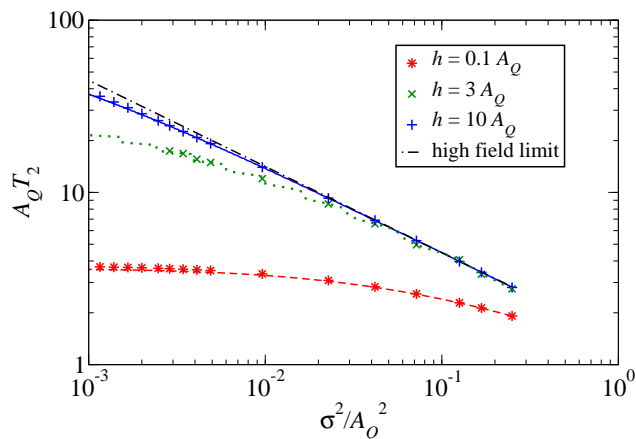


Figure 7. Coherence time T_2 for various external magnetic fields h depending on the initial variance σ^2 . The data points are calculated for $N = 49$ bath spins and nonuniform couplings with $x = 1$. The colored lines (dashed, dotted and solid) are calculated for $N = 999$ bath spins and uniform couplings. The black dash-dotted line is the curve for the effective high-field model in (47).

In the low-field regime the slope of the coherence time $T_2(\sigma^2)$ falls quickly so that T_2 does not grow strongly as σ^2 decreases. For $\sigma^2 < 0.0005A_Q$ the coherence time takes roughly double the value of $T_2(\sigma^2 = A_Q^2/4)$ for the variance without any narrowing, i.e., $\gamma = 0$. The fact that T_2 increases only weakly for lowered variance can be easily explained by the flip-flop terms. These terms are not influenced by the narrowing of the spin bath and affect the central spin equally for any value of γ . Hence the decoherence of the central spin cannot be suppressed efficiently.

In the regime of larger fields $h = 3A_Q$ and $h = 10A_Q$ we observe a different behavior in Fig. 7. The data matches the thermodynamic limit (47) well for variances $\sigma^2 \gtrsim A_Q^2/50$. For these values of the variance the coherence time T_2 is almost independent of the magnetic field h as long as the field is still large enough, i.e., the system is still in the high-field regime. The data deviates from the thermodynamic limit for lower values of σ^2 . For $h = 10A_Q$ the data agrees with the formula down to lower variances than for $h = 3A_Q$. Nonetheless, even for $h = 10A_Q$, we clearly see deviations for $\sigma^2 < A_Q^2/100$.

The coherence time for finite moderate magnetic fields grows more slowly than it does in the high-field limit. But $T_2(\sigma^2)$ continues to increase for decreasing σ^2 and it may diverge for $\sigma^2 \rightarrow 0$ even for finite fields h . This would imply that the absolute value of the correlation function in (45) does not fall below $1/e$. We have not found any signature of this scenario in the transverse spin dynamics perpendicular to a finite magnetic field. Indeed, even for vanishing initial Overhauser fluctuations the flip-flop terms cause the central spin to exchange its z -polarization with the bath. So, on one hand, $\sigma^2 = 0$ does not imply the absence of decoherence. On the other hand, we recall that rigorous arguments show that persisting correlations are generic in the CSM without magnetic field if the distribution of couplings is normalizable^{68,69}. This does not even require that $\sigma^2 = 0$ holds.

In Fig. 8, we plot the time-dependent variance $\sigma^2(t)$ for the spread parameter $x = 1$ and the narrowing factor $\gamma = 100$ to illustrate the temporal evolution of $\sigma^2(t)$. Clearly, $\sigma^2(t)$ oscillates which is mainly induced by the external magnetic field h . In addition, there is a trend to increase. We use the first maximum $\sigma_m^2(t_m)$ of the oscillations to quantify the temporal evolution in the limit of vanishing initial variance σ^2 , i.e., $\gamma \rightarrow \infty$.

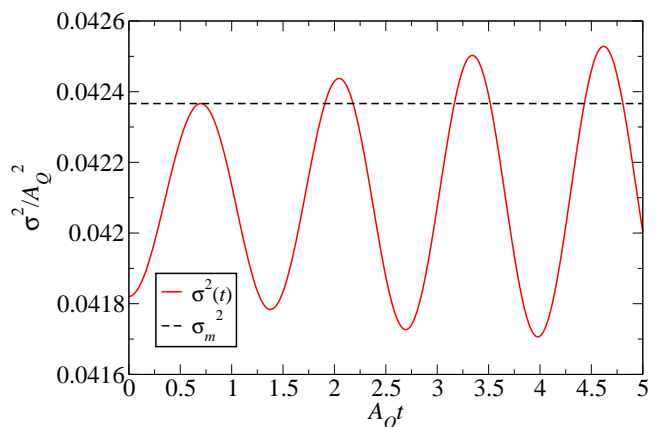


Figure 8. Time-dependent variance $\sigma^2(t)$ of the Overhauser field for nonuniform couplings with coupling spread $x = 1$ in (4), narrowing factor $\gamma = 100$, and external magnetic field $h = 5A_Q$. In addition, we plot the value of the first maximum σ_m^2 of the time-dependent variance as a black dashed line.

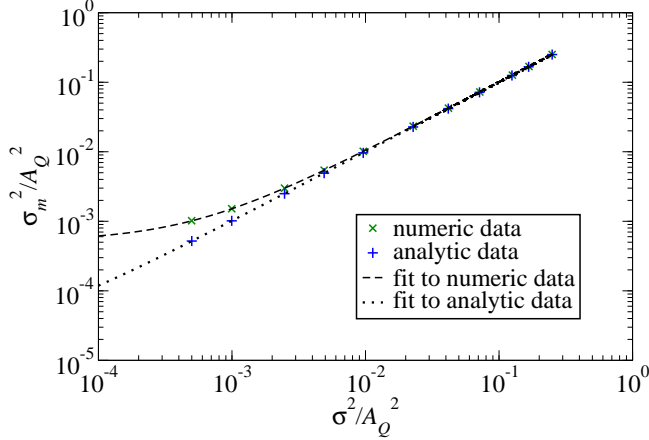


Figure 9. First maximum of the dynamic variance $\sigma^2(t)$ at time t_m , see Fig. 8, depending on the initial variance σ^2 for external magnetic field $h = 5 A_Q$. The green crosses are calculated for $N = 49$ bath spins and nonuniform couplings with $x = 1$. The dashed line is the corresponding quadratic fit. The blue crosses are calculated for $N = 999$ bath spins and uniform couplings. The dotted line is the corresponding linear fit. Both fits yield finite values of σ_m^2 for $\sigma^2 \rightarrow 0$.

In Fig. 9, we plot the value of the first maximum σ_m^2 of the time-dependent variance as a function of the initial variance σ^2 for external magnetic field $h = 5A_Q$. The curve decreases with decreasing $\sigma^2(0)$ for both uniform and nonuniform couplings. To analyze the behavior of σ_m^2 in the limit $\sigma^2 \rightarrow 0$ we fit the polynomials f_1 and f_2 which take the form

$$f_1(\sigma^2) = a_1 + b_1\sigma^2 + c_1\sigma^4 \approx \sigma_m^2(x = 1), \quad (51a)$$

$$f_2(\sigma^2) = a_2 + b_2\sigma^2 \approx \sigma_m^2(x = 0), \quad (51b)$$

to the data of the nonuniform and the uniform system, respectively. The fits are used to extrapolate the first maximum for $\sigma^2 \rightarrow 0$ yielding a_1 and a_2 . Quantitatively, these values depend on the external magnetic field. But the qualitative behavior for all finite magnetic fields h is the same. Hence it is sufficient to discuss the effect of $\sigma^2 \rightarrow 0$ for one choice $h = 5A_Q$ of the magnetic field.

Both fits yield finite values

$$a_1 = (5.15224 \cdot 10^{-4} \pm 3.192 \cdot 10^{-6}) A_Q^2 \quad (52a)$$

$$a_2 = (1.84859 \cdot 10^{-5} \pm 2.211 \cdot 10^{-8}) A_Q^2 \quad (52b)$$

for $\sigma^2 = 0$. Thus, we find the remarkable fact that the first maximum $\sigma_m(t_m)$ is finite even if the initial variance vanishes. This is shown in Fig. 9 for $h = 5A_Q$. For different magnetic fields the numeric values change but stay finite so that the qualitative finding remains the same. Note that this observation supports the above argument that the flip-flop terms induce decoherence even if the initial variance vanishes. One mechanism is that the variance is not constant and increases in the course of time even if it was zero in the beginning.

Since the fluctuations of the Overhauser field are finite for $t > 0$ the correlation in (45) decreases in time even for $\sigma^2(t = 0) \rightarrow 0$. Still the limit of a vanishing initial variance σ^2 yields the best possible reduction of decoherence. Thus we want to determine the longest possible coherence time. To this end, we conceive an extrapolation scheme to calculate the absolute correlation function $|C(t)|$ for $\sigma^2 \rightarrow 0$. As pointed out in the previous subsection the limit $\sigma^2 \rightarrow 0$ leads easily to finite size artifacts for uniform couplings. We can use even larger bath sizes N to calculate $C(t)$ for uniform couplings. The results are very similar to the corresponding results for nonuniform couplings. Hence we restrict the analysis to the correlation for nonuniform couplings with spread parameter $x = 1$. From the data we determine the dependence of $|C(t)|$ on the variance σ^2 at fixed time t . In Fig. 10, we plot $|C(t)|$ for three different fields h depending on the initial variance σ^2 . All three graphs can be approximated very well by the function

$$|C(t)| = C_0(t) \exp(-a(t)\sigma^2). \quad (53)$$

Here, the parameters $C_0(t)$ and $a(t)$ are fitted for the fixed time $t = 10/A_Q$. The resulting fits are displayed in Fig. 10 as well.

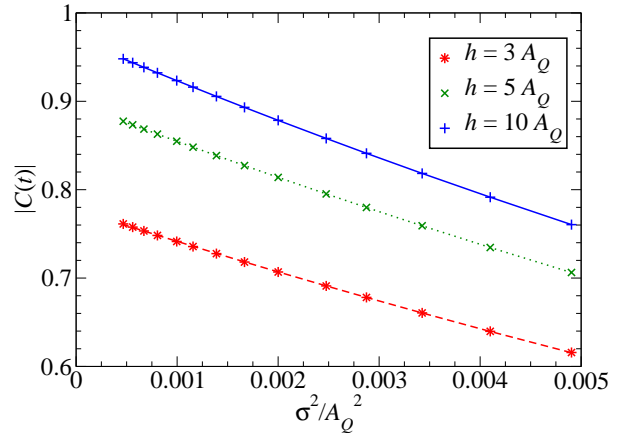


Figure 10. Absolute value of the correlation function $C(t)$ for $A_Q t = 10$ and its dependence on the variance σ^2 for three magnetic fields and nonuniform couplings with $x = 1$ in (4). The colored lines (dashed, dotted and solid) are fits of the form (53) to the data points.

For each time t we determine the parameters $C_0(t)$ and $a(t)$ in (53) by fits to the numeric data. Since we are interested in the limit $\sigma^2 \rightarrow 0$ the absolute value of the correlation $C(t)$ in this limit is given by $C_0(t)$. The prefactor $C_0(t)$ represents the correlation with the largest possible decoherence time T_2 for a given magnetic field h because the limit $\sigma^2 \rightarrow 0$ yields the best possible reduction of fluctuations of the Overhauser field.

In Fig. 11, the resulting $C_0(t)$ is displayed for three different magnetic fields h . The correlation $C_0(t)$ decreases

in time, but it does so much more slowly than for finite σ^2 . With increasing magnetic fields h the correlation decreases more and more slowly. Hence one can achieve higher coherence times T_2 in this limit as can also be seen in Fig. 7.

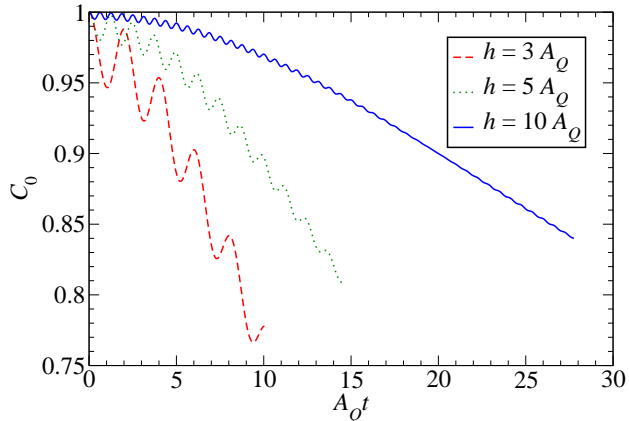


Figure 11. Fit parameter $C_0(t)$ in (53) depending on time t for three different magnetic fields h and nonuniform couplings with $x = 1$ in (4). The parameter $C_0(t)$ is equal to the absolute value of the correlation function $C(t)$ in the limit $\sigma^2 \rightarrow 0$. Hence the curves represent the correlation functions for optimally suppressed fluctuations in the spin bath and yield the maximum coherence time T_2 .

2. Dependence on the external magnetic field

In Figs. 7 and 11, we observe clearly that the decoherence of the central spin is influenced by the applied magnetic field h . In both figures, the coherence time grows with increasing magnetic field h . The solution (47) for infinite magnetic field represents the upper limit of the coherence time T_2 . Here, we focus on more details as they are relevant in any experimental setup which is described by the CSM.

We plot the coherence time T_2 as function of h for three narrowing factors γ in Fig. 12. In addition, we include the corresponding coherence time $T_{2,\infty}$ in the high-field limit from (48) for the three values of γ . Remarkably, the curve for $\gamma = 0$ behaves qualitatively different. Hence we will discuss the cases $\gamma = 0$ and $\gamma > 0$ separately.

For $\gamma = 0$, the coherence time T_2 depends hardly on the external magnetic field h . The curve overshoots the high-field limit $T_{2,\infty}$ slightly, but approaches $T_{2,\infty}$ in (48) quickly for higher fields h . This finding agrees with previous results⁵² where the CSM was analyzed as well without any narrowing. We point out that the coherence time T_2 in Ref. 52 was determined by a Gaussian fit to a different correlation function and was thus not defined in precisely the same way as in the present work. Nonethe-

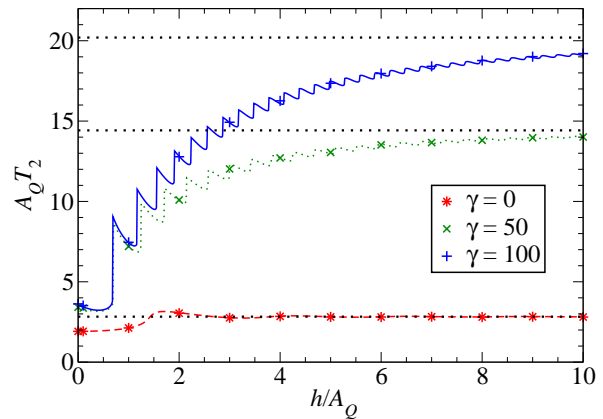


Figure 12. Coherence time T_2 as function of the external magnetic field h for various narrowing factors γ . The data points are calculated for $N = 49$ bath spins and nonuniform couplings with $x = 1$ in (4). The colored lines (dashed, dotted and solid) are calculated for $N = 999$ bath spins and uniform couplings. The dotted black lines are the corresponding coherence times $T_{2,\infty}$ in (48) for the three values of γ in the high-field limit $h \rightarrow \infty$.

less, the results are qualitatively the same. Also Ref. 44 showed that for sufficiently large fields the decoherence of the system is independent of the magnetic field.

In contrast to the curve without narrowing, the two curves for $\gamma = 50$ and $\gamma = 100$ show an overall increase of the coherence time T_2 with growing magnetic field h besides the sawtooth features which we explained at the beginning of this subsection. The coherence time T_2 does not increase without bound, but it converges to the value $T_{2,\infty}$. The physics is easily explained. By increasing the magnetic field the influence of the flip-flop terms of the Hamiltonian in (1b) is decreased. Then, the fluctuations of the Overhauser field become the main source of decoherence. Since we narrow the distribution of the Overhauser field, i.e., we reduce the detrimental fluctuations the coherence time can be increased. This works efficiently for high magnetic fields because at low fields the flip-flop mechanism is still at work inducing decoherence which is unrelated to the initial variance σ^2 .

This observation allows us also to establish a connection to the common distinction between longitudinal relaxation and transverse relaxation or dephasing. Both processes together yield decoherence. But a sizable magnetic field is required to separate them clearly. For large field the longitudinal relaxation is reduced and suppressed in the high-field limit because transitions via the flip-flop terms are its prerequisite. Then, decoherence reduces to pure dephasing. For moderate magnetic fields, however, dephasing and longitudinal relaxation are both at work. For a quantitative analysis, we inspect the convergence of the coherence time T_2 for a finite field h to the infinite-

field limit $T_{2,\infty}$. This process can be assessed by the relative deviation

$$\Delta T_2 = \left| \frac{T_2}{T_{2,\infty}} - 1 \right|. \quad (54)$$

For small fields the deviation is quite large. In this regime the flip-flop terms in the Hamiltonian are still active in the dynamics of the central spin. Upon increasing field h the deviation ΔT_2 decreases and fulfills

$$\Delta T_2 \propto h^{-2} \quad \text{for } h > 5A_Q. \quad (55)$$

In this regime, the dynamics of the central spin is dominated by the $\hat{B}_z \hat{S}_z$ interaction between the central spin and the Overhauser field. Hence the fluctuations of the Overhauser field dominate the dephasing. By narrowing its initial distribution one can efficiently increase the coherence time T_2 in the high-field limit $h \gg 1A_Q$.

V. CONCLUSION

The central spin model describes a wide range of decoherence phenomena due to spin baths, for instance in quantum dots. One important proposal to reduce decoherence is to suppress the fluctuations in the bath. The key quantity is the Overhauser field, i.e., the sum of the effects of all bath spins on the central spin. Thus, the goal of our study was to investigate the effect of narrowed distributions of the Overhauser field. To this end, we used and extended two state-of-the-art techniques for the central spin model. We calculated the dynamics of the central spin for large spin baths by numeric DMRG for nonuniform distribution of couplings and by an analytic solution for uniform couplings.

By introducing the narrowing factor γ we adjusted the initial variance σ^2 of the Overhauser field. The narrowing factor γ and σ^2 are related by a one-to-one mapping, i.e., for given values of the spread parameter x and the bath size N the variance is determined by γ . Our study revealed that the initial variance depends only slightly on the spread parameter x and on the bath size N for a wide range of parameters.

We showed that generally the coherence time T_2 of the central spin model can be increased substantially by narrowing the distribution of Overhauser field. There is, however, an important restriction to this statement. The

coherence time does not grow upon decreasing the variance σ^2 of the Overhauser field independent of the applied magnetic field. Without field, the narrowing is almost pointless. Our results extend previous findings^{29,33} dealing with high magnetic fields. Only in this limit, the relation $T_2 \propto 1/\sigma$ is valid.

For low magnetic fields the coherence time $T_2(\sigma)$ is limited roughly by twice the value $T_2(\sigma_0)$ without any narrowing. The dynamics is driven by the flip-flop terms which are unchanged by narrowing the distribution of the Overhauser field. Hence the coherence of the central spin decays quite fast even for very small values of σ^2 . Therefore, the coherence time is almost independent on σ^2 for narrowly distributed Overhauser fields.

With increasing magnetic field the coherence time increases because the flip-flop terms are suppressed more and more. Nonetheless, the coherence time increases more slowly than the inverse of σ . In addition, we showed that the central spin decoheres even in the limit of vanishing initial variance σ^2 because the flip-flop terms are still active.

In the high-field regime, the system can be approximated by an effective Hamiltonian containing no flip-flop terms^{70,71}. In hole-doped systems, the flip-flop terms are reduced from the beginning⁴²⁻⁴⁴. Without the flip-flop terms, the coherence time is indeed inversely proportional to σ . Hence T_2 can be increased arbitrarily by decreasing σ . But the coherence time is bounded for the cases where flip-flop terms are present.

The initial variance σ^2 of the Overhauser field determines the maximum coherence time of the central spin system. This can be achieved for optimum conditions, i.e., for very large magnetic field applied to the central spin. The role of the external magnetic field is to suppress the effect of the flip-flop terms.

Further research in this field, for instance the investigation of other distributions of the couplings or the effect of protocols of dynamic decoupling, is certainly called for. Our study has illustrated that time dependent density-matrix renormalization is a very useful numeric tool to this end.

VI. ACKNOWLEDGMENT

We thank the Deutsche Forschungsgemeinschaft for financial support in project UH90/9-1 and in the ICRC TRR 160 together with the Russian Foundation of Basic Research.

* lars.gravert@tu-dortmund.de

¹ D. Loss and D. P. DiVincenzo, Phys. Rev. A **57**, 120 (1998).

² I. A. Merkulov, A. L. Efros, and M. Rosen, Phys. Rev. B **65**, 205309 (2002).

³ A. V. Khaetskii, D. Loss, and L. Glazman, Phys. Rev. Lett. **88**, 186802 (2002).

⁴ J. M. Kikkawa and D. D. Awschalom, Phys. Rev. Lett. **80**, 4313 (1998).

⁵ A. Greulich, R. Oulton, E. A. Zhukov, I. A. Yugova, D. R. Yakovlev, M. Bayer, A. Shabae, A. L. Efros, I. A.

- Merkulov, V. Stavarache, *et al.*, Phys. Rev. Lett. **96**, 227401 (2006).
- ⁶ R. Hanson, L. P. Kouwenhoven, J. R. Petta, S. Tarucha, and L. M. K. Vandersypen, Rev. Mod. Phys. **79**, 1217 (2007).
- ⁷ A. Greilich, D. R. Yakovlev, A. Shabaev, A. L. Efros, I. A. Yugova, R. Oulton, V. Stavarache, D. Reuter, A. Wieck, *et al.*, Science **313**, 341 (2006).
- ⁸ A. Greilich, A. Shabaev, D. R. Yakovlev, A. L. Efros, I. A. Yugova, D. Reuter, A. D. Wieck, and M. Bayer, Science **317**, 1896 (2007).
- ⁹ A. Greilich, M. Wiemann, F. G. G. Hernandez, D. R. Yakovlev, I. A. Yugova, M. Bayer, A. Shabaev, A. L. Efros, D. Reuter, and A. D. Wieck, Phys. Rev. B **75**, 233301 (2007).
- ¹⁰ X. Xu, Y. Wu, B. Sun, Q. Huang, J. Cheng, D. G. Steel, A. S. Bracker, D. Gammon, C. Emary, and L. J. Sham, Phys. Rev. Lett. **99**, 097401 (2007).
- ¹¹ J. Schliemann, A. Khaetskii, and D. Loss, J. Phys.: Condens. Matter **15**, R1809 (2003).
- ¹² L. Viola and S. Lloyd, Phys. Rev. A **58**, 2733 (1998).
- ¹³ W. M. Witzel and S. Das Sarma, Phys. Rev. Lett. **98**, 077601 (2007).
- ¹⁴ G. S. Uhrig, Phys. Rev. Lett. **98**, 100504 (2007).
- ¹⁵ H. Uys, M. J. Biercuk, and J. J. Bollinger, Phys. Rev. Lett. **103**, 040501 (2009).
- ¹⁶ M. J. Biercuk, H. Uys, A. P. VanDevender, N. Shiga, W. M. Itano, and J. J. Bollinger, Nature **458**, 996 (2009).
- ¹⁷ J. Du, X. Rong, N. Zhao, Y. Wang, J. Yang, and R. B. Liu, Nature **461**, 1265 (2009).
- ¹⁸ C. Barthel, J. Medford, C. M. Marcus, M. P. Hanson, and A. C. Gossard, Phys. Rev. Lett. **105**, 266808 (2010).
- ¹⁹ H. Bluhm, S. Foletti, I. Neder, M. Rudner, D. Mahalu, V. Umansky, and A. Yacoby, Nature Phys. **7**, 109 (2010).
- ²⁰ G. de Lange, Z. H. Wang, D. Ristè, V. V. Dobrovitski, and R. Hanson, Science **330**, 60 (2010).
- ²¹ A. Imamoglu, E. Knill, L. Tian, and P. Zoller, Phys. Rev. Lett. **91**, 017402 (2003).
- ²² M. Gullans, J. J. Krich, J. M. Taylor, H. Bluhm, B. I. Halperin, C. M. Marcus, M. Stopa, A. Yacoby, and M. D. Lukin, Phys. Rev. Lett. **104**, 226807 (2010).
- ²³ M. J. A. Schuetz, E. M. Kessler, L. M. K. Vandersypen, J. I. Cirac, and G. Giedke, Phys. Rev. B **89**, 195310 (2014).
- ²⁴ S. E. Economou and E. Barnes, Phys. Rev. B **89**, 165301 (2014).
- ²⁵ D. S. Smirnov, Phys. Rev. B **91**, 205301 (2015).
- ²⁶ W. A. Coish and D. Loss, Phys. Rev. B **70**, 195340 (2004).
- ²⁷ A. S. Bracker, E. A. Stinaff, D. Gammon, M. E. Ware, J. G. Tischler, A. Shabaev, A. L. Efros, D. Park, D. Gershoni, V. L. Korenev, *et al.*, Phys. Rev. Lett. **94**, 047402 (2005).
- ²⁸ J. Baugh, Y. Kitamura, K. Ono, and S. Tarucha, Phys. Rev. Lett. **99**, 096804 (2007).
- ²⁹ D. Stepanenko, G. Burkard, G. Giedke, and A. Imamoglu, Phys. Rev. Lett. **96**, 136401 (2006).
- ³⁰ D. Klauser, W. A. Coish, and D. Loss, Phys. Rev. B **73**, 205302 (2006).
- ³¹ J. Danon and Y. V. Nazarov, Phys. Rev. Lett. **100**, 056603 (2008).
- ³² M. Issler, E. M. Kessler, G. Giedke, S. Yelin, I. Cirac, M. D. Lukin, and A. Imamoglu, Phys. Rev. Lett. **105**, 267202 (2010).
- ³³ A. R. Onur and C. H. van der Wal, ArXiv e-prints (2014), 1409.7576.
- ³⁴ C. Latta, A. Högele, Y. Zhao, A. N. Vamivakas, P. Maletinsky, M. Kroner, J. Dreiser, I. Carusotto, A. Badolato, D. Schuh, *et al.*, Nature Phys. **5**, 758 (2009).
- ³⁵ I. T. Vink, K. C. Nowack, F. H. L. Koppens, J. Danon, Y. V. Nazarov, and L. M. K. Vandersypen, Nature Phys. **5**, 764 (2009).
- ³⁶ X. Xu, W. Yao, B. Sun, D. G. Steel, A. S. Bracker, D. Gammon, and L. J. Sham, Nature **459**, 1105 (2009).
- ³⁷ H. Bluhm, S. Foletti, D. Mahalu, V. Umansky, and A. Yacoby, Phys. Rev. Lett. **105**, 216803 (2010).
- ³⁸ S. Lee, P. von Allmen, F. Oyafuso, G. Klimeck, and K. B. Whaley, J. Appl. Phys. **97**, 043706 (2005).
- ³⁹ M. Y. Petrov, I. V. Ignatiev, S. V. Poltavtsev, A. Greilich, A. Bauschulte, D. R. Yakovlev, and M. Bayer, Phys. Rev. B **78**, 045315 (2008).
- ⁴⁰ M. Gaudin, J. Phys. France **37**, 1087 (1976).
- ⁴¹ M. Gaudin, *La Fonction d'Onde de Bethe* (Masson, Paris, 1983).
- ⁴² J. Fischer, W. A. Coish, D. V. Bulaev, and D. Loss, Phys. Rev. B **78**, 155329 (2008).
- ⁴³ C. Testelin, F. Bernardot, B. Eble, and M. Chamarro, Phys. Rev. B **79**, 195440 (2009).
- ⁴⁴ J. Hackmann and F. B. Anders, Phys. Rev. B **89**, 045317 (2014).
- ⁴⁵ J. Hackmann, P. Glasenapp, A. Greilich, M. Bayer, and F. B. Anders, Phys. Rev. Lett. **115**, 207401 (2015).
- ⁴⁶ M. Bortz and J. Stolze, J. Stat. Mech. **2007**, P06018 (2007).
- ⁴⁷ W. A. Coish, D. Loss, E. A. Yuzbashyan, and B. L. Altshuler, J. Appl. Phys. **101**, 081715 (2007).
- ⁴⁸ A. Faribault and D. Schuricht, Phys. Rev. Lett. **110**, 040405 (2013).
- ⁴⁹ A. Faribault and D. Schuricht, Phys. Rev. B **88**, 085323 (2013).
- ⁵⁰ A. Friedrich, *Time-dependent Properties of one-dimensional Spin-Systems: a DMRG-Study* (PhD thesis, RWTH Aachen, 2006).
- ⁵¹ D. Stanek, C. Raas, and G. S. Uhrig, Phys. Rev. B **88**, 155305 (2013).
- ⁵² D. Stanek, C. Raas, and G. S. Uhrig, Phys. Rev. B **90**, 064301 (2014).
- ⁵³ M. Bortz, S. Eggert, C. Schneider, R. Stübner, and J. Stolze, Phys. Rev. B **82**, 161308(R) (2010).
- ⁵⁴ B. Erbe and J. Schliemann, Phys. Rev. Lett. **105**, 177602 (2010).
- ⁵⁵ F. T. Arecchi, E. Courtens, R. Gilmore, and H. Thomas, Phys. Rev. A **6**, 2211 (1972).
- ⁵⁶ S. R. White, Phys. Rev. Lett. **69**, 2863 (1992).
- ⁵⁷ U. Schollwöck, Rev. Mod. Phys. **77**, 259 (2005).
- ⁵⁸ U. Schollwöck, Ann. of Phys. **326**, 96 (2011).
- ⁵⁹ S. R. White and A. E. Feiguin, Phys. Rev. Lett. **93**, 076401 (2004).
- ⁶⁰ A. J. Daley, C. Kollath, U. Schollwöck, and G. Vidal, J. Stat. Mech. **2004**, P04005 (2004).
- ⁶¹ A. Bühler, N. Elstner, and G. S. Uhrig, Eur. Phys. J. B **16**, 475 (2000).
- ⁶² C. Karrasch, J. H. Bardarson, and J. E. Moore, Phys. Rev. Lett. **108**, 227206 (2012).
- ⁶³ M. B. Hatano and M. Suzuki, Lect. Notes Phys. **678**, 37 (2005).
- ⁶⁴ P. Schmitteckert, Phys. Rev. B **70**, 121302 (2004).
- ⁶⁵ L. Cywiński, Acta Phys. Pol. A **119**, 576 (2011).
- ⁶⁶ D. Gobert, C. Kollath, U. Schollwöck, and G. Schütz, Phys. Rev. E **71**, 036102 (2005).

- ⁶⁷ A. Braun and P. Schmitteckert, Phys. Rev. B **90**, 165112 (2014).
⁶⁸ G. S. Uhrig, J. Hackmann, D. Stanek, J. Stolze, and F. B. Anders, Phys. Rev. B **90**, 060301(R) (2014).
⁶⁹ U. Seifert, P. Bleicker, P. Schering, A. Faribault, and G. S. Uhrig, ArXiv e-prints (2016), 1603.08894.
⁷⁰ W. M. Witzel and S. Das Sarma, Phys. Rev. B **74**, 035322 (2006).
⁷¹ F. H. L. Koppens, D. Klauser, W. A. Coish, K. C. Nowack, L. P. Kouwenhoven, D. Loss, and L. M. K. Vandersypen, Phys. Rev. Lett. **99**, 106803 (2007).

Appendix A: Time evolution for uniform couplings

For uniform couplings in the CSM (1b) we can calculate the time evolution analytically. We have to calculate the time evolution for states of the form $|\uparrow\rangle \otimes |j, m\rangle$ and $|\downarrow\rangle \otimes |j, m\rangle$. As argued in Sec. III A the Hamiltonian in (1b) is block diagonal for uniform couplings, thus, the time evolution can be calculated fairly easily because the blocks are of dimension two only. For the following calculation, we shift the Hamiltonian by $A_Q/\sqrt{N}4$ leading to

$$\hat{H}' = \frac{A_Q}{\sqrt{N}} \hat{\mathbf{I}}\hat{\mathbf{S}} - h\hat{S}_z + \frac{A_Q}{4\sqrt{N}}. \quad (\text{A1})$$

This shift has no influence on expectation values of the system because it cancels out in the traces. For the two states $|1\rangle = |\uparrow\rangle |j, m\rangle$ and $|2\rangle = |\downarrow\rangle |j, m+1\rangle$ with $|m| < j$ the effect of the Hamiltonian is

$$\hat{H}' |1\rangle = a_m |1\rangle + b_{j,m} |2\rangle, \quad (\text{A2a})$$

$$\hat{H}' |2\rangle = -a_m |2\rangle + b_{j,m} |1\rangle, \quad (\text{A2b})$$

where we use the abbreviations

$$a_m = \frac{(2m+1)}{4} \frac{A_Q}{\sqrt{N}} - h/2, \quad (\text{A3a})$$

$$b_{j,m} = \frac{A_Q}{2\sqrt{N}} \sqrt{(j-m)(j+m+1)}. \quad (\text{A3b})$$

Diagonalizing the block matrices yields the eigenvalues

$$\omega_{j,m}^\pm = \pm \sqrt{a_m^2 + b_{j,m}^2} \quad (\text{A4})$$

of \hat{H}' . With them the time evolution is given by

$$|1\rangle(t) = (c_{j,m} - i s_{j,m}) |1\rangle - i \tilde{s}_{j,m} |2\rangle, \quad (\text{A5a})$$

$$|2\rangle(t) = (c_{j,m} + i s_{j,m}) |2\rangle - i \tilde{s}_{j,m} |1\rangle, \quad (\text{A5b})$$

where we employ the abbreviations

$$c_{j,m} = \cos(\omega_{j,m} t), \quad (\text{A6a})$$

$$s_{j,m} = \sin(\omega_{j,m} t) \frac{a_m}{\omega_{j,m}}, \quad (\text{A6b})$$

$$\tilde{s}_{j,m} = \sin(\omega_{j,m} t) \frac{b_{j,m}}{\omega_{j,m}}. \quad (\text{A6c})$$

Two states are left out so far, namely $|+\rangle := |\uparrow\rangle |j, j\rangle$ and $|-\rangle := |\downarrow\rangle |j, -j\rangle$. They are eigenstates of \hat{H}' and can be evolved in time directly yielding

$$|\pm\rangle(t) = \exp\left[-i\left(\frac{A_Q(2j+1)}{4\sqrt{N}} \pm \frac{h}{2}\right)t\right] |\pm\rangle. \quad (\text{A7})$$

The last step is to calculate the expectation values $\sigma^2(t)$ in (32) and $C(t)$ in (45). For a lighter notation we define the weighted sums

$$\overline{f_{j,m}} := \sum_{j,m} g_{j,m}(\gamma) f_{j,m}. \quad (\text{A8})$$

The weight $g_{j,m}$ is defined in (15). The maximum of j is $j_{\max} = N/2$ while its minimum is $j_{\min} = 0$ or $j_{\min} = 1/2$ for an even or odd N , respectively. The quantum number m ranges from $-j$ to j . and the range of the indices j and m is given in Sec. III A.

For the variance $\sigma^2(\gamma)$ we need to calculate two expectation values. With the help of the time evolved states we obtain

$$\langle \hat{B}_z \rangle = \frac{A_Q}{\sqrt{N}} \left(\overline{m} + \overline{\tilde{s}_{j,m}^2} \right) \quad (\text{A9a})$$

$$\langle \hat{B}_z^2 \rangle = \frac{A_Q^2}{N} \left(\overline{m^2} + \overline{(2m+1) \tilde{s}_{j,m}^2} \right) \quad (\text{A9b})$$

by taking the traces. Since the narrowing of the distribution of the Overhauser field is symmetric with respect to the quantum number m , the weighted sum \overline{m} vanishes. For the initial variance σ^2 in (33) we obtain the simpler result

$$\sigma^2 = \frac{A_Q^2}{N} \overline{m^2} \quad (\text{A10})$$

because all terms proportional to $\sin(\omega_{j,m} t)$ vanish. Thus, we dispose of the expressions to calculate the initial variance σ^2 and the time dependent variance $\sigma^2(t)$. To find the correlation function $C(t)$, we need to compute only one expectation value. Using the given time evolution of states we obtain the solutions for the real and imaginary parts of $C(t)$

$$\Re[C(t)] = \overline{c_{j,m} c_{j,m-1}} - \overline{s_{j,m} s_{j,m-1}}, \quad (\text{A11a})$$

$$\Im[C(t)] = \overline{c_{j,m} s_{j,m-1}} + \overline{s_{j,m} c_{j,m-1}}. \quad (\text{A11b})$$

Appendix B: Computing the narrowed state by DMRG

In Sec. III B we discussed how one can realize the narrowed Overhauser fields by DMRG. Here we present further details. The task is to construct the narrowed state $|\gamma\rangle$ by evaluating

$$|\gamma\rangle = \exp\left(-\frac{\gamma}{2} \hat{B}_z^2 / A_Q^2\right) |\psi\rangle = \hat{M} |\psi\rangle. \quad (\text{B1})$$

The state $|\psi\rangle$ is the purified state as introduced previously in Ref. 51.

We can easily apply the exponential operator \hat{M} in (B1) by expressing the purified state $|\psi\rangle$ in the eigenbasis of the Overhauser field \hat{B}_z , see below. In DMRG, the purified state $|\psi\rangle$ is approximated by a state in the product basis of the system block S and the environment block E after each DMRG step of a sweep, including the truncation of the basis. In the following, vectors of the system block will be denoted by the subscript S and vectors of the environment block by the subscript E . For more details regarding the steps and sweeps the reader is referred to Ref. 51.

After a step of the sweep, we can express the state $|\psi\rangle$ in the truncated product basis of system and environment by

$$|\psi\rangle = \sum_{i,j} \Psi_{ij} |i\rangle_S |j\rangle_E \quad (\text{B2})$$

with the coefficients Ψ_{ij} and the vectors $|i\rangle_S$ and $|j\rangle_E$. In the DMRG algorithm we express the narrowed state also as the purified state in the same basis, i.e., we use

$$|\gamma\rangle = \sum_{i,j} \Gamma_{ij} |i\rangle_S |j\rangle_E. \quad (\text{B3})$$

In order to calculate the coefficients Γ_{ij} , one applies the exponential function \hat{M} in (B1) to the purified state $|\psi\rangle$. Note that the Overhauser field naturally splits into the part $\hat{B}_{z,S}$ from the system block and $\hat{B}_{z,E}$ from the environment block so that $\hat{B}_z = \hat{B}_{z,S} + \hat{B}_{z,E}$. We denote the eigenvectors of $\hat{B}_{z,S}$ by $|a\rangle_S$ with eigenvalues λ_a and those of $\hat{B}_{z,E}$ by $|b\rangle_E$ with eigenvalues μ_b . Then, the action of \hat{M} amounts to

$$\hat{M} |a\rangle_S |b\rangle_E = \exp\left[-\frac{\gamma}{2} (\lambda_a + \mu_b)^2 / A_Q^2\right] |a\rangle_S |b\rangle_E. \quad (\text{B4})$$

In order to re-express a purified state from a DMRG step in terms of the eigenbasis of $\hat{B}_{z,S}$ and $\hat{B}_{z,E}$ we perform the following transformation. Let us assume that the state is first given in the truncated basis resulting from the DMRG step denoted by $|c\rangle_S$ and $|d\rangle_E$. The eigenbasis of $\hat{B}_{z,S}$ and $\hat{B}_{z,E}$ is denoted by $|a\rangle_S$ and $|b\rangle_E$. Then, the desired coefficients of $|\psi\rangle$ are computed according to

$$\Psi'_{ab} = \sum_{c,d} {}_S \langle a | c \rangle_S {}_E \langle b | d \rangle_E \Psi_{cd}. \quad (\text{B5})$$

The exponential operator \hat{M} can be straightforwardly applied to the state in the eigenbasis of $\hat{B}_{z,S}$ and $\hat{B}_{z,E}$. This state is transformed back to the original truncated basis yielding the coefficients

$$\Gamma_{ij} = \sum_{a,b} {}_S \langle i | a \rangle_S {}_E \langle j | b \rangle_E M_{ab} \Psi'_{ab}. \quad (\text{B6})$$

These coefficients provide the target state $|\gamma\rangle$ we need for the next DMRG step.

Appendix C: Choice of weights

In Sec. III B, we described that the narrowed state $|\gamma\rangle$ can be constructed more accurately by adding two additional density matrices

$$\hat{\rho}_1 = \text{Tr}_E \left[\hat{B}_z |\psi\rangle \langle \psi | \hat{B}_z \right], \quad (\text{C1a})$$

$$\hat{\rho}_2 = \text{Tr}_E \left[\hat{B}_z |\gamma\rangle \langle \gamma | \hat{B}_z \right] \quad (\text{C1b})$$

to the reduced density matrix $\hat{\rho}'_S$ in (24). The state $|\psi\rangle$ is the initial purified state without narrowing. The weighted sum

$$\hat{\rho}_S = w_0 \hat{\rho}'_S + w_1 \hat{\rho}_1 + w_2 \hat{\rho}_2 \quad (\text{C2})$$

is used to define the basis truncation in the DMRG step. Clearly, $\hat{\rho}_S$ depends on the choice of the normalized weights w_0 , w_1 , and w_2 .

To analyze the influence of the weights we define the relative error of the partition function Z

$$\Delta Z(w_1, w_2) = \left| \frac{Z_n(w_1, w_2)}{Z_a} - 1 \right| \quad (\text{C3})$$

between the data calculated by DMRG and the analytic solution, see (25) and (14). We fix the parameter $\gamma = 50$ and the bath size $N = 49$, but we checked that for other sets of γ and N the error ΔZ displays the same qualitative behavior. Hence we restrict ourselves to this exemplary set.

In Fig. 13, $\Delta Z(w_2)$ is displayed for two values of w_1 . Since the sum of the weights is unity the value of w_0 is implicitly determined for the data points. The plot shows that for $w_1 = 0$ or $w_2 = 0$ the error is relatively large. The green data (crosses) is calculated for $w_1 = 0$; the relative error lies at about 10^{-7} for most values of w_2 . The red data (asterisks) lies at about 10^{-11} for $w_1 = 0.1$ and almost all values of w_2 . For different values $w_1 > 0$ the corresponding error ΔZ is of the same order of magnitude. We conclude that one can choose the weights relatively freely to obtain reliable results. But the total exclusion of one of the extra density matrices has to be avoided. If this rule of thumb is complied with, the additional error introduced by the time evolution dominates. This case was studied elaborately in Ref. 51.

Appendix D: Accuracy check for the DMRG data

Here we present a more detailed analysis of the accuracy of the DMRG calculations. The analytic solutions for uniform couplings serve as benchmarks for this analysis. During the build-up of the narrowed state $|\gamma\rangle$ we can easily calculate the partition function Z_n according to (25). This result is compared to the analytic solution in (14). For quantitative comparison, we define the relative error

$$\Delta Z(\gamma, N) = \left| \frac{Z_n(\gamma, N)}{Z_a(\gamma, N)} - 1 \right| \quad (\text{D1})$$

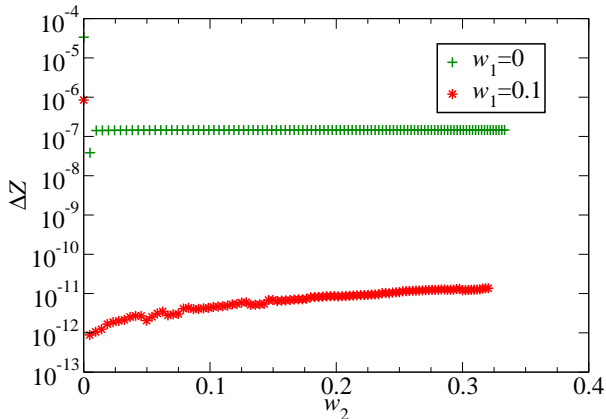


Figure 13. Relative error $\Delta Z(w_2)$ for two values of the weight w_1 .

of the partition function Z between the data calculated by DMRG and the analytic data, see (25) and (14). The error depends on the narrowing factor γ as well as on the bath size N .

In Fig. 14, we show $\Delta Z(\gamma)$ for $N = 49$ and $N = 50$. Since the partition function behaves quite differently for odd and even values of N data for both cases is included. For all values of γ , the error ΔZ is below 10^{-9} and for most values even below 10^{-11} . We cannot identify a clear dependence of ΔZ on the narrowing factor γ , but we observe that the error is very small for all considered values of γ .

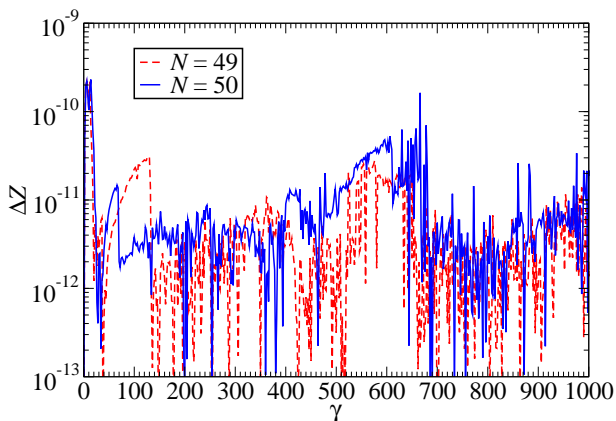


Figure 14. Relative error $\Delta Z(\gamma)$ as function of γ .

Figure 15 shows the dependence of $\Delta Z(N)$ on the bath size N for $\gamma = 200$. The relative error is again below 10^{-9} for all values of N . For larger bath sizes, we observe an increase of the error roughly proportional to N^2 . Since

we consider mostly $N = 49$ in the calculations presented in the main text the increase of the error is not an issue. Additionally, the prefactor of the power law N^2 is of the order of 10^{-14} . This means that one can treat large systems reliably by DMRG if desired.

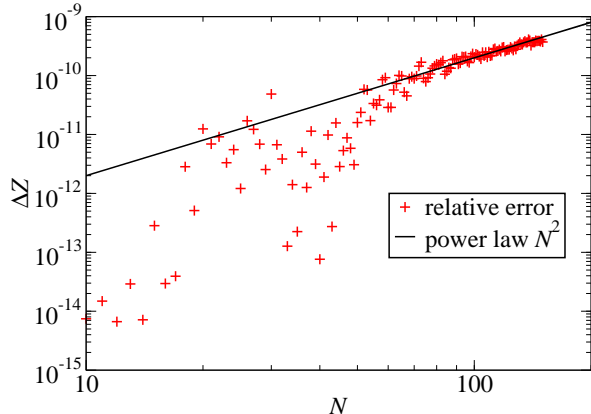


Figure 15. Relative error $\Delta Z(N)$ as function of N .

In summary, the DMRG approach to create narrowed states is remarkably accurate. For time dependent quantities, the additional error due to the Trotter-Suzuki decomposition is dominating. This error has been comprehensively analyzed before⁵¹.

Appendix E: Thermodynamic limit

We study uniform and nonuniform couplings in systems with large bath size N . If we consider $N \rightarrow \infty$, the central limit theorem helps us to express the tedious sums in the partition function Z in (8) by a much simpler integral

$$Z(\gamma) \approx Z_\infty(\gamma) := \frac{2^N}{\sqrt{2\pi\sigma_0}} \int_{-\infty}^{\infty} e^{-\frac{B_z^2}{2\sigma_0^2}} e^{-\gamma \frac{B_z^2}{A_Q^2}} dB_z \quad (\text{E1})$$

with the variance $\sigma_0^2 = A_Q^2/4$ in (39) of the Overhauser field for $\gamma = 0$ and the classical Overhauser field B_z , see Ref. 2 for more details regarding this limit. The partition function Z_∞ denotes this thermodynamic limit.

Since the variance σ_0^2 is independent on the precise distribution of the couplings the result Z_∞ is valid for uniform and nonuniform couplings. The limit Z_∞ can be calculated analytically yielding

$$Z_\infty(\gamma) = \frac{2^{N+1}}{\sqrt{4+2\gamma}}. \quad (\text{E2})$$

The corresponding variance $\sigma_\infty^2(\gamma)$ of the Overhauser field results from (35) and we find

$$\sigma_\infty^2(\gamma) = \frac{A_Q^2}{4+2\gamma}. \quad (\text{E3})$$

In this way, we can describe the initial variance of the Overhauser field in the thermodynamic limit. By comparing (E3) with numeric results we investigated the finite size effects of the system for various coupling spreads x and bath sizes N .

Appendix F: High-field limit

For an infinitely large external magnetic field an analytic solution for the correlation function (45) of the central spin exists. The derivation is similar to the calculation in Refs. 2 and 65, but we extend the previous result to narrowed distributions of Overhauser fields.

In the high-field limit $h \gg A_Q$ the Hamiltonian \hat{H} in (1b) can be approximated by an effective Hamiltonian \hat{H}_{eff} of the form

$$\hat{H}_{\text{eff}} = \hat{B}_z \hat{S}_z - h \hat{S}_z, \quad (\text{F1})$$

neglecting terms which change \hat{S}_z because their effect vanishes proportional to $1/h$. Hence the flip-flop terms vanish⁷¹. In addition, we consider the limit $N \rightarrow \infty$ to make use of the central limit theorem. Combining both limits, the correlation function $C(t)$ in (45) reduces to

$$C(t) \approx C_\infty(t) := \frac{2^N e^{iht}}{\sqrt{2\pi\sigma_0} Z_\infty(\gamma)} I \quad (\text{F2})$$

with the variance $\sigma_0^2 = A_Q^2/4$ in (39) of the Overhauser field for $\gamma = 0$ and the partition function $Z_\infty(\gamma)$. The integral I reads

$$I := \int_{-\infty}^{\infty} \exp\left(-\frac{B_z^2}{2\sigma_0^2} - \gamma \frac{B_z^2}{A_Q^2} - iB_z t\right) dB_z \quad (\text{F3})$$

with the classical Overhauser field B_z . It can be calculated analytically

$$C_\infty(t) = \exp\left(-\frac{\sigma_\infty^2(\gamma)t^2}{2} + iht\right) \quad (\text{F4})$$

for the correlation function in the thermodynamic limit. The initial variance $\sigma_\infty^2(\gamma)$ in (E3) is the variance in the thermodynamic limit.

Since we define the coherence time T_2 by $|C(T_2)| = 1/e$ we easily obtain the relation

$$T_{2,\infty} := \frac{\sqrt{2}}{\sigma_\infty} \quad (\text{F5})$$

for the coherence time in the high-field limit.